https://doi.org/10.1016/j.tws.2023.110571

Numerical investigation on local buckling behaviour of cold-formed high strength steel irregular hexagonal hollow section stub columns

Jun-zhi Liu[1,a]; Han Fang[2]; Tak-Ming Chan[3,4] *

[1] School of National Safety and Emergency Management, Beijing Normal University, China

[a] Formerly, Department of Civil and Environmental Engineering, The Hong Kong Polytechnic University, Hong Kong, China

[2] School of Civil Engineering, University of Leeds, United Kingdom

[3] Department of Civil and Environmental Engineering, The Hong Kong Polytechnic University, Hong Kong, China

[4] Chinese National Engineering Research Centre for Steel Construction (Hong Kong Branch), The Hong Kong Polytechnic University, Hong Kong, China

* Corresponding author: tak-ming.chan@polyu.edu.hk

Abstract

The local buckling behaviour of cold-formed high strength steel (HSS) irregular hexagonal hollow section (IHexHS) stub columns under concentric compression is studied numerically in this paper. Finite-element (FE) models were developed and validated against the experimental data. The validated FE models were employed to conduct extensive parametric studies. The obtained numerical results together with the experimental data were used to evaluate the applicability of the existing design codes and design approaches to the cold-formed HSS IHexHS under concentric compression. The evaluation shows that the current slenderness yield limit values codified in design codes cannot be applied to cold-formed HSS IHexHS stub columns. The Eurocode 3 (EC3) and the North American code AISC 360-16 provide slightly over-estimated predictions for slender sections whereas the Australian code AS 4100 yields conservative predictions. For stocky sections, all the design codes show high degree of conservatism due to the lack of consideration for strain hardening. Furthermore, design approaches of Continuous Strength Method (CSM) and Generalised Slenderness Resistance Method (GSRM) have been found to provide more accurate predictions than the Direct Strength Method (DSM). Modified design approaches are also proposed to improve the accuracy of the strength predictions.

Keywords: High strength steel; Local buckling behaviour, Cold-forming effect; Irregular hexagonal hollow section stub columns; Numerical modelling; design approaches.

1. Introduction

The application of cold-formed high strength steel (HSS) hollow section structures can be observed in various construction sectors including buildings, bridges, offshore platforms, nuclear, thermal plants as well as the pipelines and pressure vessels [1]. The HSS can be produced with acceptable ductility and weldability due to the advancements in material technology and welding techniques. The general tendency of using higher strength steel can be observed in the construction industry due to the high strength-to-weight ratio which enables the use of lighter structural components with reduced member sizes as well as decreased costs such as the transportation fees for using trucks and lifting apparatuses [2].

In order to implement the structural components made from high strength steel plates, numerous research studies have been conducted to investigate the structural performance of the welded and cold-formed HSS hollow section members subject to realistic loading conditions. In the past years, research efforts have been made with the focus on conventional tubular members such as the welded box sections [3–17], and open sections [18–22] under different loading conditions. In addition to the welded sections, hot-rolled (hot-finished) sections of SHS and RHS have also been studied focusing on the local buckling behaviour at cross-sectional level [22–27]. Unlike the welded sections and hot-finished sections, cold-formed HSS hollow sections are becoming increasingly popular due to their simple fabrication route, less energy consumption, as well as the improved strength induced by cold-rolling or press-braking. Additionally, experimental investigations have been conducted on cold-formed HSS tubular sections including common sections of square hollow sections (SHS), rectangular hollow sections (RHS) and circular sections (CHS) [28–35].

In recent years, the newly emerged structural systems, such as the modular integrated construction (MIC) or the modular steel buildings (MSB), propose higher requirement on the versatility of the structural configurations and connection possibilities. Numerous innovative cross-section types have been developed and investigated including elliptical hollow sections (EHS) [36-42] and semi-oval hollow sections (SOHS) [43-46]. In recent years, increasing interests have also been made focusing on the applications of polygonal sections such as HSS hexagonal hollow sections (HexHS) [47, 48], irregular hexagonal hollow sections (IHexHS) [49, 50], octagonal hollow sections (OctHS) [51, 52] and irregular octagonal hollow sections (IOctHS) [53, 54]. Compared with traditional profile and other innovative sections, HexHS/IHexHS and OctHS/IOctHS feature combined advantages of the higher buckling resistance and easier connection options with incoming members. The flat surface of the HexHS/IHexHS and OctHS/IOctHS can provide a platform for operators to conduct welding or bolted-connection with T-stub or gusset plate in comparison to CHS or EHS, whereas better local buckling resistance can be realised due to the relatively shorter flat width than that of SHS and RHS if they are delivered with similar perimeters [55–56]. Moreover, the application of the above-mentioned polygonal sections can be formed into the composite columns by infilling the concrete, being employed as mega column members in high-rise or long-span structures with heavy loads [50]. Despite the illustrated prominent advantages of HexHS/IHexHS, limited studies have been performed at material, cross-section and member level for HSS HexHS/IHexHS, underlying the necessities to further systematically explore the structural behaviour of those sections. The material property variations, residual stress distributions and local buckling behaviour, have been experimentally investigated for HSS cold-formed HexHS with sections made of Q690 steel grade (nominal yield strength f_y = 690 MPa in [47, 48]. Existing experimental investigation into cold-formed HSS IHexHS can only be found in [49, 50], which present the structural behaviour at cross-sectional level under concentric compression.

To better understand the structural behaviour and promote the application of HSS IHexHS, numerical investigations of local buckling performance of cold-formed HSS IHexHS are presented in this paper. The numerical investigation presented in this paper are primarily based upon the experimental study on 20 HSS cold-formed IHexHS stub columns with large spectrum of cross-section dimensions (b/t) varying from 3.8 to 34.5. The finite element (FE) models were firstly developed and validated against the collected test results [50]. Further to the numerical modelling, extensive parametric studies were conducted to generate more structural performance data to supplement the test data pool, encompassing a larger spectrum of cross-sectional slenderness and steel grades. The obtained ultimate resistances under concentric compression were used to assess the suitability of the existing design provisions for structural steels stipulated in EN 1993-1-1 [59] EN

1993-1-5 [60], EN 1993-1-12 [61], AISI/AISC 360-16 [62] and AS 4100 [63] and design approaches of Direct Strength Method (DSM), Continuous Strength Method (CSM), and Generalised Slenderness Resistance Method (GSRM). It is noteworthy that the design specifications for internal plate members were assessed. Although HSS design are allowed in these codes, limitations are provided for HSS tubular sections. Specifically, hollow sections with nominal yield strength not greater than 485 MPa and 450 MPa are allowed to be designed in AISI/AISC 360-16 and AS 4100.

2. Numerical investigation

2.1. General

A comprehensive numerical investigation to be presented in the following sections includes the finite-element modelling programme, validation, and parametric studies. The finite-element (FE) models were developed using the commercially available software package of ABAQUS [64]. The FE model was firstly developed to replicate the structural performance obtained from experiments reported by Liu et al. [50] for HSS cold-formed IHexHS stub columns under concentric compression. In [50], a total of 20 Q690 HSS cold-formed IHexHS stub column specimens with two nominal plate thicknesses of 6 mm and 10 mm under axial compression were tested. The experimental set-up of the stub column tests with instrumentation is presented in Fig. 1. The notations defining the geometries of each cold-formed HSS IHexHS stub column are illustrated in Fig. 2, where H is the height of the cross section, B is the outer width of the IHexHS, B_L is the longer edge length of the IHexHS, b_L is the clear width of the vertical flat portion with welding bead excluding the corner regions, B_s is the shorter edge length, b_s is the clear width of an inclined short flat side excluding the corner portions, t is the nominal thickness of the cross section, r_o and r_i are the outer and inner corner radius of the cross section respectively. Subsequently, extensive parametric studies were carried out to generate additional structural performance data on cold-formed HSS IHexHS stub columns with various cross-sectional slenderness and steel grades under concentric compression.

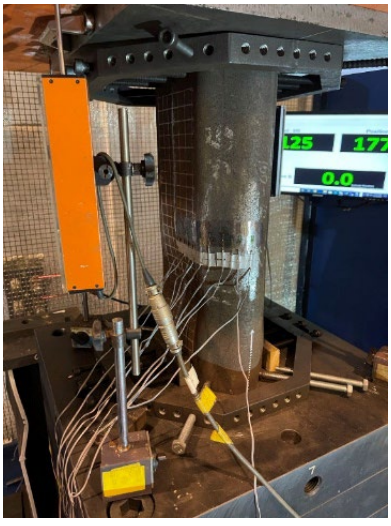

Fig. 1. Experimental instrumentation for cold-formed HSS IHexHS stub columns under concentric compression.

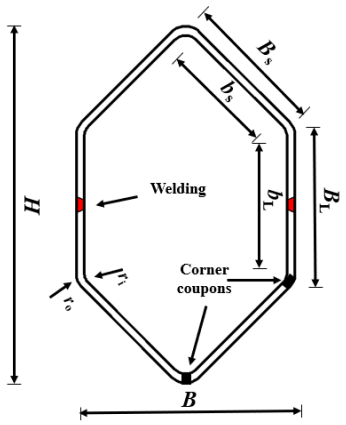

Fig. 2. Cross section of the HSS cold-formed irregular hexagonal hollow sections.

2.2. FE modelling

This section presents the FE modelling techniques developed for HSS cold-formed IHexHS stub columns. Key information including the element selection, boundary conditions, mesh size, initial local geometric imperfections, cold-forming effect, and residual stress effect are discussed and evaluated. The four-noded shell element with reduced integration (S4R) was employed in modelling HSS cold-formed IHexHS stub columns, which have been successfully applied in FE modelling to predict the structural responses of various hollow sections structures with different cross-sectional shapes [54, 66]. In accordance with the preliminary mesh sensitivity studies, the mesh size was selected with a uniform value of $b_s/20$ for the flat portions and a finer mesh of $b_s/30$ was assigned to the corner portions to explicitly account for the curved geometry, balancing the prediction accuracy with reasonable computational cost.

To accurately predict the structural behaviour of the modelled specimens, measured geometries and engineering stress-strain relationships for HSS IHexHS were used, as summarised in Table 1. Material properties were assigned through the entries available in ABAQUS with elastic and plastic properties modules. The recorded Young's modulus E_s, and Poisson's ratio of 0.3, were incorporated in the elastic range, while the measured non-linear stress-strain material properties from the flat coupons and the corner coupons were converted to the true stress and logarithmic plastic strain following Eqs. (1) – (2) respectively, and then incorporated in plastic range. Plastic material model with isotropic hardening was used for modelling the HSS materials [67, 68].

$$\sigma_{\text{true}} = \sigma_{\text{eng}}(1+\varepsilon_{\text{eng}}) \tag{1}$$

$$\varepsilon_{\text{true}}^{\text{pl}} = \ln(1+\varepsilon_{\text{eng}}) - (\frac{\sigma_{\text{true}}}{E_s}) \tag{2}$$

where σ_{eng} and ε_{eng} are the engineering stress and engineering strain from tensile coupon tests, E_s is Young's modulus obtained from the tests, and σ_{true} and $\varepsilon_{\text{true}}^{\text{pl}}$ are the true stress and plastic strain.

As it was observed that the material strength at corner regions of the HSS cold-formed IHexHS was strengthened through tensile coupon tests due to the strain hardening from press-braking effect, this effect should be explicitly taken into account for accurate structural analysis. Therefore, the enhanced material strengths were incorporated into the corner portions by assigning the measured stress-strain relationships to the corner portions of the FE models. Previous studies also found that the enhancement of the strength was not

152 Table 1 Summary of the tensile coupon test results.

Specimen	Flat coupon					Corner coupon				
	E	f_y	f_u	ε_f	ε_u	E_c	$f_{y,c}$	$f_{u,c}$	$\varepsilon_{f,c}$	ε_u
	(GPa)	(N/mm^2)	(N/mm^2)	(%)	(%)	(GPa)	(N/mm^2)	(N/mm^2)	(%)	(%)
IHex-70×6-1.45-90	217.1	767	809	14.3	6.1	197.7	825	871	10.6	1.7
IHex-70×6-1.45-135	-[a]	-[a]	-[a]	-[a]	-[a]	198.6	823	853	10.4	1.8
IHex-70×6-1.50-90	203.5	776	818	16.1	6.5	195.4	818	862	11.3	1.5
IHex-70×6-1.50-135	-[a]	-[a]	-[a]	-[a]	-[a]	197.3	815	854	10.6	1.8
IHex-70×6-1.55-90	211.2	772	822	15.6	6.1	195.6	806	858	9.6	1.5
IHex-70×6-1.55-135	-[a]	-[a]	-[a]	-[a]	-[a]	199.8	807	822	10.2	1.5
IHex-70×6-1.60-90	198.1	774	816	15.8	6.6	193.7	812	857	9.8	1.7
IHex-70×6-1.60-135	-[a]	-[a]	-[a]	-[a]	-[a]	201.3	820	869	11.5	2.5
IHex-125×6-1.80-90	206.5	768	825	16.1	6.4	200.2	814	865	10.9	1.6
IHex-125×6-1.80-135	-[a]	-[a]	-[a]	-[a]	-[a]	198.3	806	856	11.6	1.7
IHex-125×6-1.60-90	205.1	773	824	16.4	6.5	199.9	819	872	10.5	1.5
IHex-125×6-1.60-135	-[a]	-[a]	-[a]	-[a]	-[a]	209.3	808	860	10.2	1.6
IHex-150×6-1.80-90	204.6	772	821	16.3	6.6	192.2	843	898	10.8	1.6
IHex-150×6-1.80-135	-[a]	-[a]	-[a]	-[a]	-[a]	195.6	840	885	12.3	1.8
IHex-160×6-1.90-90	211.2	775	825	15.6	6.7	202.7	821	868	11.5	1.5
IHex-160×6-1.90-135	-[a]	-[a]	-[a]	-[a]	-[a]	208.3	809	847	10.8	1.5
IHex-165×6-1.85-90	201.2	777	829	14.8	6.2	208.7	805	851	10.9	1.6
IHex-165×6-1.85-135	-[a]	-[a]	-[a]	-[a]	-[a]	201.3	801	845	11.5	1.8
IHex-185×6-2.15-90	224.4	782	836	17.6	6.4	203.5	827	880	11.6	1.7
IHex-185×6-2.15-135	-[a]	-[a]	-[a]	-[a]	-[a]	202.0	818	871	12.1	1.9
IHex-185×6-1.90-90	213.1	772	828	15.3	6.6	201.5	822	885	12.2	1.8
IHex-185×6-1.90-135	-[a]	-[a]	-[a]	-[a]	-[a]	198.5	819	876	11.5	1.6
IHex-225×6-2.15-90	211.7	780	831	17.2	6.4	196.2	818	868	12.2	1.7
IHex-225×6-2.15-135	-[a]	-[a]	-[a]	-[a]	-[a]	195.6	809	849	13.5	1.6
IHex-150×10-1.70-90	211.1	776	817	16.3	5.8	198.8	802	845	11.9	1.9

IHex-150×10-1.70-135	-[a]	-[a]	-[a]	-[a]	-[a]	199.5	810	863	13.1	1.8
IHex-160×10-1.50-90	206.5	775	826	15.3	6.2	197.5	824	879	10.5	1.6
IHex-160×10-1.50-135	-[a]	-[a]	-[a]	-[a]	-[a]	203.5	821	878	10.6	1.7
IHex-170×10-2.00-90	202.6	779	827	16.3	6.5	198.5	825	872	10.2	1.8
IHex-170×10-2.00-135	-[a]	-[a]	-[a]	-[a]	-[a]	202.4	822	871	11.8	1.9

Note: [a] denotes the material properties are the same as the specimen with the same designation apart from the numerical suffix.

limited to the corner portion only, and it can be extended to a distance away from the corner based on the experimental observations. The extended corner regions with a width of 2*t* were used by Gardner and Nethercot [69] for cold-formed stainless steel SHS/RHS, 3*t* for HSS SHS/RHS by Ma et al. [30], and 1.5*t* for HSS OctHS by Chen et al. [51]. The investigated cold-formed HSS IHexHS in this study featured with different cold-bent corners of 90° and 135°, the tensile coupon results reported in Liu et al. [49] imply that the effect of the cold-bent angle on material properties and residual stresses was minimal. Hence, the applicability and suitability of the corner extension for IHexHS was assessed simultaneously for both 90° and 135°corners. Sensitivity study was performed to investigate the effect of the extension of the corner region with schematic view as shown in Fig. 3. It is shown that the assignment of material properties from flat and corner coupons to flat portion and corner portion without extension yield close agreement with the test results as shown in Table 2 with mean value of the normalised resistance between numerical value to the tested one $N_{u,FE}/N_{u,test} = 1.01$ with coefficient of variation CoV = 0.03, similar to the findings in previous studies in Singh et al. [70]. Thus, in this study, the enhanced strength was assigned to the corresponding corner portions only without any further extension.

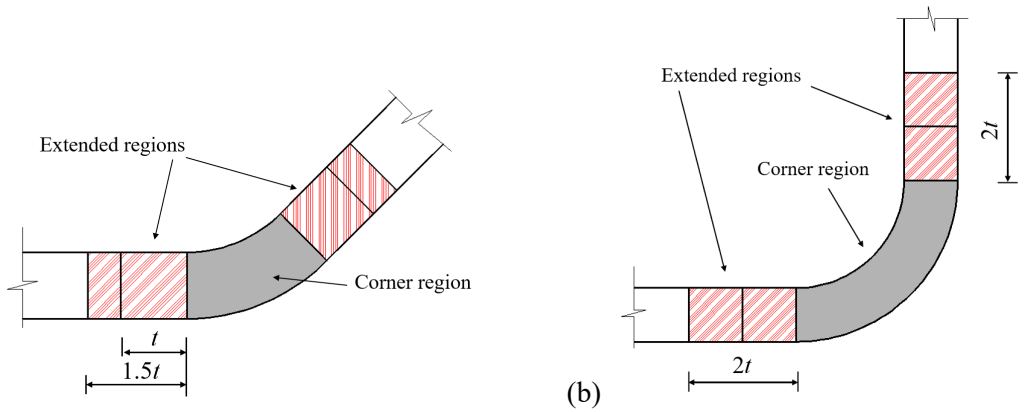

Fig. 3. Extension of the corner regions in cold-formed HSS IHextHS finite element model (a) Corner extensions for HSS cold-formed IHexHS corner with angle of 135 degree (b) Corner extensions for HSS cold-formed IHexHS corner with angle of 90 degree.

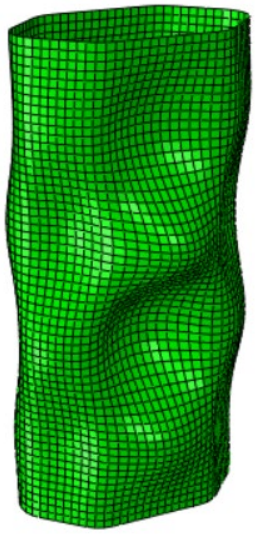

Fig. 4. Typical first buckling mode shape generated from Eigenvalue analysis

Initial imperfection are important parameters influencing the structural performance and ultimate resistance, which are introduced to the structural components during transportation, fabrication, erection and storage. Linear elastic buckling analysis was carried out and the lowest elastic buckling eigenmode was selected as the representative local geometric imperfection profile. Measured initial local geometric imperfection magnitude was used and scaled to the corresponding imperfection profile from linear perturbation, as shown in Fig. 4.

Furthermore, to simulate the fix-ended boundary conditions concord with the experimental set-up, the reference points were constrained to the nodes at the edges of the end sections through kinematic coupling constraints. The reference points were restrained against all other degree of freedoms, except for the longitudinal displacement at the reference point on the loading side. Displacement-control loading employed in experiments was simulated by assigning the displacement in longitudinal direction in the RIKS step. Non-linear geometric option of (*NLGEOM) was activated to allow for large displacement analysis. Typical loading and boundary conditions of the cold-formed HSS IHexHS stub columns under concentric compression is shown in Fig. 5.

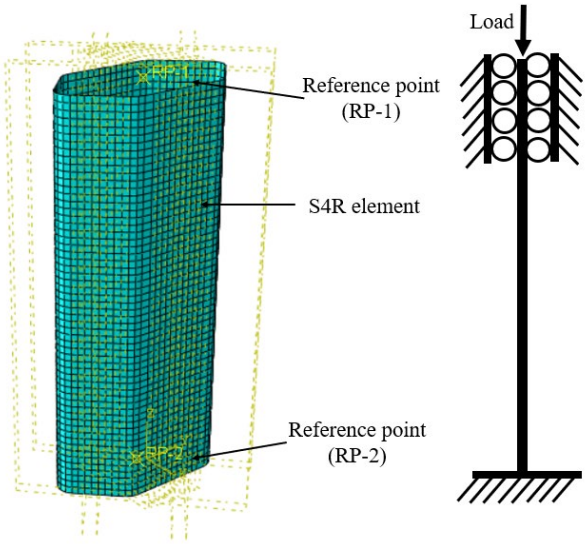

Fig. 5. Typical FE mesh, loading and boundary conditions of the cold-formed HSS IHexHS stub columns.

The fabrication processes of cold-forming (press-braking) and welding generate inter-lock residual stresses in initial state prior to the external loading being applied to the specimens. The effect of the residual stresses should be accounted for in the FE modelling. The residual stresses can be decomposed into membrane and bending residual stresses. The bending residual stresses were inherently reintroduced during the straightening of the slightly curved coupon specimen during tensile coupon tests. Thus, the bending residual stresses were essentially included in the stress-strain relationship measured from the coupon specimens cut within the cross-sections of the specimens [52, 54]. Thereafter, the effect of the residual stresses on the structural response of the model was considered by incorporating the membrane residual stresses into the FE model with the magnitudes from the predictive model for HSS cold-formed IHexHS proposed in [49], as shown in Fig. 6. Typical initial stress distribution after incorporating the membrane residual stresses in the FE model is depicted in Fig. 7, with positive values indicating tensile membrane residual stress and negative values indicating compressive membrane residual stress.

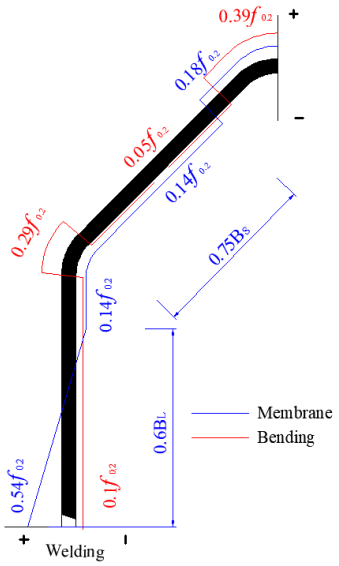

Fig. 6. Predictive model of membrane and bending residual stresses distributions and amplitudes (in MPa) in modelled cold-formed HSS IHextHS stub columns [49].

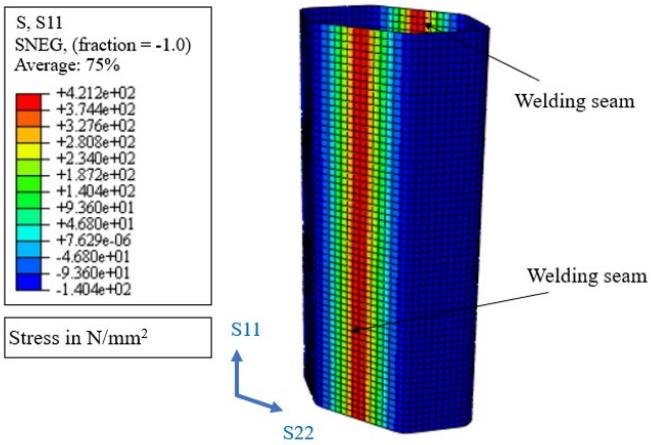

Fig. 7. Typical membrane and bending residual stresses distributions in the modelled cold-formed HSS cold-formed IHextHS stub column specimen of IHex-150×6-1.80.

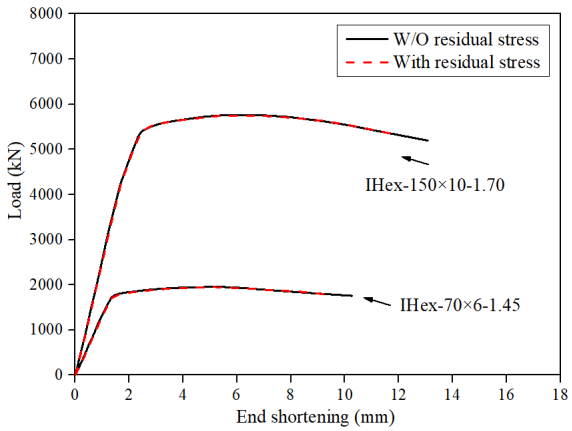

(a)

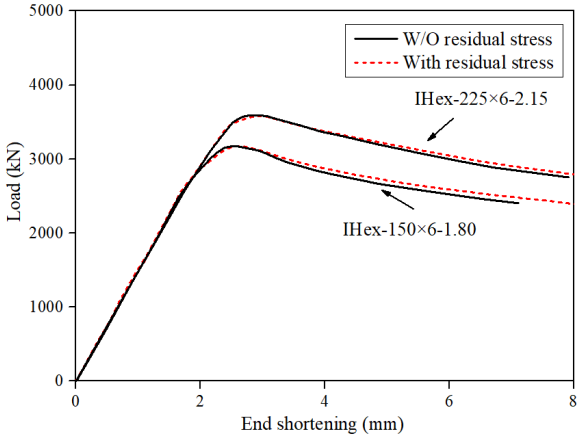

(b)

Fig. 8. Comparison of FE models of cold-formed HSS IHexHS stub columns with and without explicit inclusion of residual stresses (a) Stocky sections of IHex-70×6-1.45 and IHex-150×10-1.70 (b) Slender sections of IHex-150×6-1.80 and IHex-225×6-2.15

2.3. Validation

The accuracy of the developed FE models was validated by comparing the obtained results in terms of load-end shortening relationships, failure modes, and ultimate resistances with those obtained from the experimental results. The FE results of axial load-end shortening curves for five representative (including slender sections and compact sections) HSS cold-formed IHexHS stub columns, which areIHex-70×6-1.45, IHex-125×6-1.60, IHex-150×6-1.80, IHex-225×6-2.15 and IHex-150×10-1.70, were compared with the those from the experimental results.

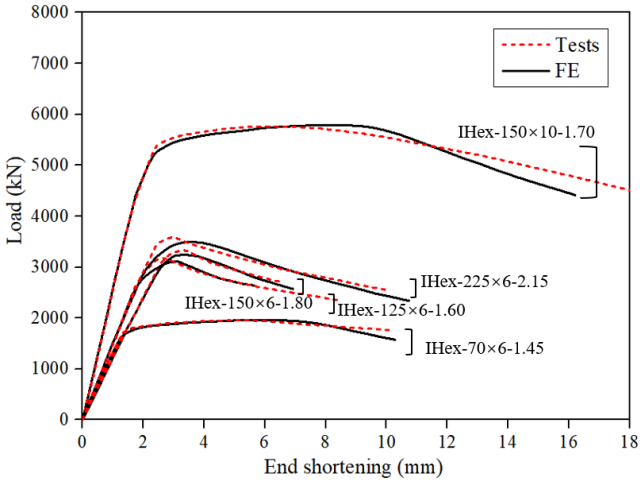

Fig. 9. Comparison of experimental and numerical load-end shortening responses of typical cold-formed HSS IHexHS stub columns.

In addition to the measured initial local geometric imperfections for IHexHS stub columns, imperfection sensitivity analysis was executed to determine the proper magnitude of the imperfection incorporated to the model, (i) the measured imperfection value ω_0 (ii) $t/100$ (iii) $t/50$ (iv) $t/10$. The sensitively analysis of the cross-sectional ultimate resistance to initial local geometric imperfection was performed by comparing the ultimate loads estimated from FE models incorporating different local imperfection amplitudes with those from the stub column tests, as presented in Table. 2. Mean values of the ratios of $N_{u,FE}/N_{u,test}$ for the four investigated initial local imperfection magnitudes are 1.01, 1.03, 1.02 and 1.01 respectively with corresponding CoVs of 0.03, 0.02, 0.02 and 0.03 respectively. The best agreement between the experimental and numerical predictions was achieved when the imperfection amplitude equal to $t/10$

The FE models without inclusion of the membrane residual stress were also modelled to compare and illustrate the necessities to incorporate the membrane residual stresses in FE model. The minimal difference within 2% was found in the ultimate capacities indicating the inclusion for the membrane residual stress is unnecessary due to its negligible effect on the structural response, as seen in Table 2. The graphical comparison of the load-end shortening curves also demonstrates the minimal effect of membrane residual stresses for cold-formed HSS IHexHS stub columns as shown in Fig. 8(a) for stocky sections and Fig. 8(b) for slender sections. The comparison also underlines that the effect of membrane residual stresses has relatively larger effect on slender

sections than stocky sections, primarily attributed to the fact that the stress re-distribution after entering into the plasticity within the stocky sections.

It is shown in Fig. 9 that the deformation curves predicted from the developed FE models can precisely capture the cross-sectional ultimate resistances. The curves of load-end shortening between FE and test correlate well each other. Moreover, the FE models were also able to replicate the failure modes of the HSS cold-formed IHexHS, as shown in Fig. 10. The failure modes in the form of local buckling generated from the FE model agreed well with the test observations for IHexHS stub column specimens. Close agreement on the ultimate resistances was also obtained with comparative values, with the statistical analysis reported in Table 2. Overall, the developed FE models can successfully replicate the failure modes and accurately predict the ultimate resistance of the cold-formed HSS IHexHS stub columns with satisfactory agreements in load-end shortening responses.

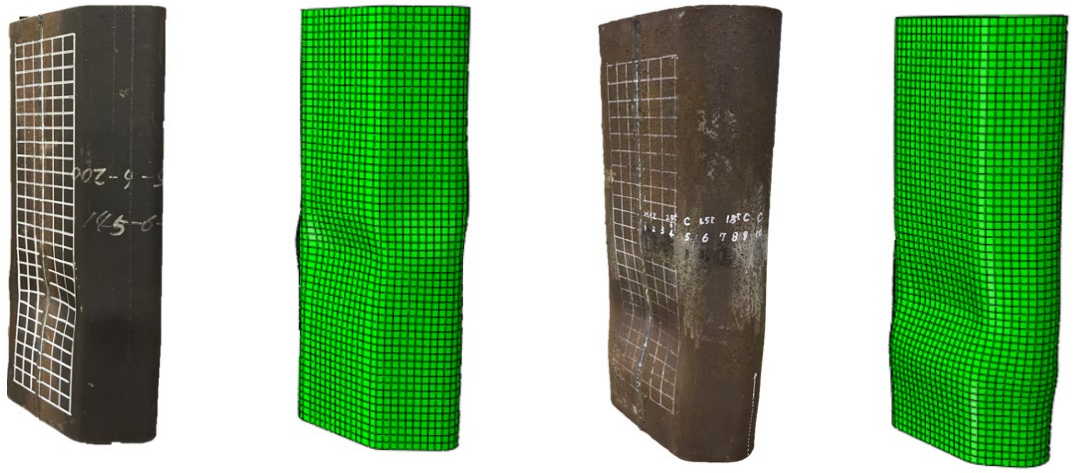

(a) (b)

Fig. 10. Test and FE failure modes for typical stub column specimen (a) Cold-formed HSS IOctHS stub column specimen IHex-150×6-1.80 (b) Cold-formed HSS IOctHS stub column specimen IHex-170×10-2.00.

2.4. Parametric studies

Following the validation of the FE models, extensive parametric studies on cold-formed HSS IHexHS stub columns were carried out to further generate structural performance data covering a larger spectrum of cross-sectional slenderness and wider range of steel grades to enhance the data pool.

The full stress-strain curves for steel materials Q460, Q690, and S960 with nominal yield strength of 460 MPa, 690 MPa and 960 MPa measured in Chen et al. [58], Liu et al. [49] and Wang et al. [65] were used. The average material properties were used with the key material properties adopted in parametric study for both flat and corner portions reported in Table 3, including the Young's modulus E_s, the yield strength f_y, the ultimate strength f_u, and the ultimate strain ε_u. The subscripts of "f" and "c" denote the flat and corner portions of the cross-sections. The stress-strain curves for specimens with nominal yield strength of 460 MPa and 690 MPa were generated based on the proposed predictive stress-strain models given in Chen et al. [58] and Liu et al. [49] whereas the measured curves were used for sections with steel grade with nominal yield strength of 960 MPa. The stress-strain curves of the cold-formed HSS IHexHS employed in parametric studies for both flat

and corner portions respectively are plotted in Fig. 11.

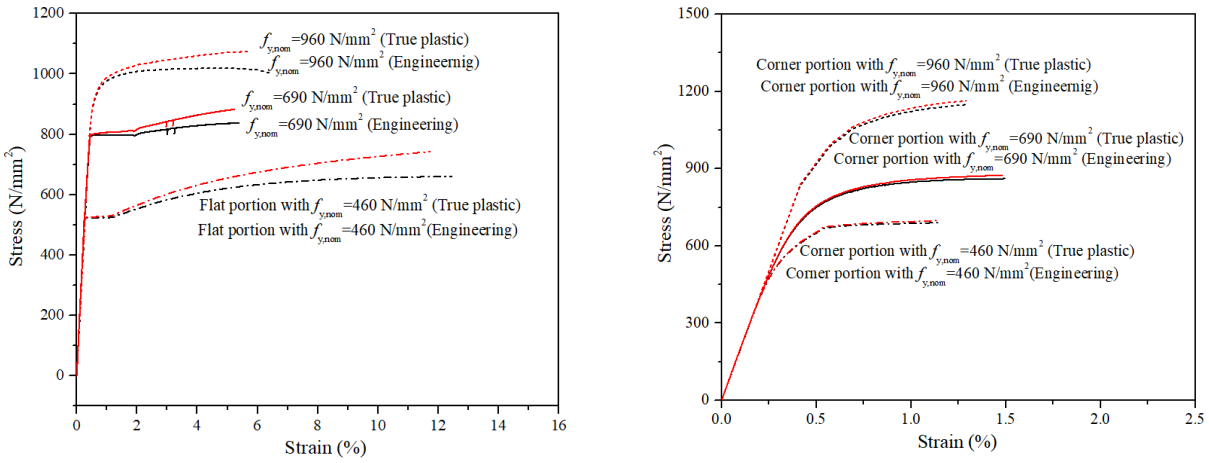

(a) (b)

Fig. 11. Engineering and true stress-strain curves of cold-formed HSS IHexHS stub columns employed in parametric study (a) Stress-strain curves of flat portions (b) Stress-strain curves of corner portions.

The investigations for cold-formed HSS SHS columns carried out by Somodi and Kovesdi [85] demonstrate that there are no clear tendencies depending on the steel grade for imperfection magnitude and the adopted initial local geometric imperfection value for steel grades among S235 to S960 was 0.7b/1000 which is independent of the steel grade, hence initial geometric imperfection value of t/10 was used in parametric studies.

The length of all the specimens were designed as 2.5 times the largest cross-section dimensions, which were deemed to be short enough to avoid interaction effect from global buckling but sufficiently long to contain the representative initial local geometric imperfection and residual stresses. In accordance with the design guideline from Ziemian [88], the length of the tested stub column specimen is suggested to be three times the largest the largest width of the cross-section for SHS/RHS. However, the IHexHS itself is characterised with different bending stiffness in different bending axis, which may be susceptible to global buckling around its minor axis, particularly for sections with a higher aspect ratio. Hence, prior numerical analysis and sensitivity study was carried out by authors to determine suitable length among 3, 2.5, and 2 times the largest cross-sectional width of IHexHS. It was found that all HexHS specimens with the length of 3 times the largest cross-sectional width failed by global buckling in all case (with global imperfection among L/1000, L/500, and L/250), whereas no global failure is observed for sections with the length taken as 2.5 times the largest cross-sectional width. The specimens lengths are thereafter designed as 2.5 times the largest cross-section dimensions. The thickness of the modelled IHexHS was kept constant as 6 mm, and the inner corner radius of the cold-bent corner of each specimen r_i was taken equal to three times of its nominal thickness. In terms of the geometric dimensions, the clear width of the longer flat portion b_L and shorter inclined flat portion b_s were varied from 48 mm to 300 mm for sections with aspect ratio of 1.0. As for sections with nominal aspect ratio of 1.5 and 2.0, the clear width of the shorter inclined flat portion b_s varied between 35 mm and 200 mm for sections with aspect ratio of 1.5, and between 24 mm and 150 mm for sections with aspect ratio of 2.0, resulting in a wider cross-section slenderness of b_s varied between 1.9 and 28.8 and b_L ranging between 8.3 and 28.8. A total of 1350 FE models were conducted in the parametric studies.

Table 2 Comparison of the experimental and numerical results.

Specimen	Cross-section	$N_{u,FE}/N_{u,test}$				$N_{u,FE}/N_{u,test}$			$N_{u,FE}/N_{u,test}$	
		Imperfection amplitudes				Corner extension imp=ω_0			Membrane residual stress	
		ω_0	t/100	t/50	t/10	Without	Extended to t	Extended to 1.5t	Yes imp=ω_0	No imp=ω_0
IHex-70×6-1.45	IHexHS	1.03	1.05	1.03	1.01	1.03	1.04	1.05	1.01	1.03
IHex-70×6-1.50	IHexHS	1.00	1.03	1.00	0.99	1.00	1.02	1.03	0.98	1.00
IHex-70×6-1.50#	IHexHS	1.00	1.03	1.00	1.00	1.00	1.02	1.03	0.98	1.00
IHex-70×6-1.55	IHexHS	1.01	1.04	1.01	1.00	1.01	1.03	1.04	1.00	1.01
IHex-70×6-1.55#	IHexHS	1.01	1.03	1.01	1.00	1.01	1.03	1.04	0.99	1.01
IHex-70×6-1.60	IHexHS	1.01	1.05	1.03	1.01	1.01	1.04	1.05	0.99	1.01
IHex-125×6-1.80	IHexHS	1.02	1.04	1.03	1.02	1.02	1.04	1.04	1.00	1.02
IHex-125×6-1.80#	IHexHS	1.02	1.04	1.03	1.02	1.02	1.04	1.04	1.01	1.02
IHex-125×6-1.60	IHexHS	1.04	1.06	1.05	1.04	1.04	1.06	1.06	1.03	1.04
IHex-150×6-1.80	IHexHS	1.02	1.03	1.02	1.02	1.02	1.04	1.04	1.02	1.02
IHex-160×6-1.90	IHexHS	1.05	1.06	1.05	1.05	1.05	1.05	1.05	1.05	1.05
IHex-160×6-1.90#	IHexHS	1.05	1.06	1.05	1.05	1.05	1.05	1.05	1.05	1.05
IHex-165×6-1.85	IHexHS	1.05	1.07	1.05	1.05	1.05	1.06	1.06	1.05	1.05
IHex-185×6-2.15	IHexHS	1.06	1.08	1.06	1.06	1.06	1.07	1.07	1.06	1.06
IHex-185×6-1.90	IHexHS	1.01	1.03	1.01	1.01	1.01	1.02	1.02	1.01	1.01
IHex-225×6-2.15	IHexHS	1.03	1.05	1.03	1.03	1.03	1.04	1.04	1.03	1.03
IHex-225×6-2.15#	IHexHS	1.04	1.06	1.04	1.04	1.04	1.04	1.04	1.04	1.04
IHex-150×10-1.70	IHexHS	1.00	1.02	1.00	0.98	1.00	1.02	1.02	0.99	1.00
IHex-160×10-1.50	IHexHS	1.02	1.04	1.02	1.00	1.02	1.03	1.03	1.00	1.02
IHex-170×10-2.00	IHexHS	1.00	1.03	1.00	0.97	1.00	1.02	1.02	0.98	1.00
	Mean	1.01	1.03	1.02	1.01	1.01	1.02	1.03	1.00	1.01
	CoV	0.03	0.02	0.02	0.03	0.03	0.02	0.02	0.03	0.03

Table 3 Key material properties adopted in parametric study.

References	Steel grade	Flat portion				Corner portion			
		E_s (N/mm^2)	f_y (N/mm^2)	f_u (N/mm^2)	ε_u (%)	$E_{s,c}$ (N/mm^2)	$f_{y,c}$ (N/mm^2)	$f_{u,c}$ (N/mm^2)	$\varepsilon_{u,c}$ (%)
Liu et al. [49]	Q460	213900	581	669	11.7	198200	735	776	1.33
Chen et al. [58]	Q690	210000	770	825	6.5	200000	815	845	1.75
Wang et al. [65]	S960	204500	946	1007	5.5	204000	1033	1174	2.50

3. Evaluation of the existing design methods

3.1 General

In this section, the applicability of the design provisions stipulated in design codes of Eurocode 3, namely EN 1993-1-1 [59], EN 1993-1-5 [60], EN 1993-1-12 [61], and the North American code of ANSI/AISC 360-16 [62] as well as the Australian code of AS 4100 [63] were assessed for cold-formed HSS IHexHS stub columns under concentric compression. In addition to the design codes, newly developed design approaches of the Direct Strength Method (DSM), Continuous Strength Method (CSM) as well as General Slenderness Resistance Method (GSRM) were also considered and evaluated for their suitability to be applied for predicting the strength of cold-formed HSS IHexHS under pure compression.

3.2 Assessment on cross-section classification

In the design framework of EN 1993-1-1, the sections which can attain the yield of Af_y under compression are classified as Class 1- 3 whereas the sections failed due to local buckling prior to sectional yielding are classified as Class 4. In cross-section classification methodology in AISC 360-16 and AS 4100, the slender sections can be considered as the corresponding class as Class 4 and non-slender sections are those sections corresponding to Class 1-3 in Eurocode 3 (EC3). To take the differences of the material strengths into account, material related parameters of $\varepsilon_{EC3} = (235/f_y)^{0.5}$, $\varepsilon_{AISC} = (E/f_y)^{0.5}$, and $\varepsilon_{AS4100} = (250/f_y)^{0.5}$ are used in these three codes respectively. Different from these three codes, design standard of AISI S100 [71] and AS/NZS 4600 [72] adopt the parameter $\lambda_p = (f_y/f_{cr})^{0.5}$ as the cross-section slenderness, where f_{cr} is the elastic local buckling, global buckling and distortional buckling stress which can be determined through the numerical analysis such as finite strip software CUFSM [73] or ABAQUS [64]. For better comparison purposes, harmonization of the yield slenderness limits value from design codes and design approaches were made that the normalised plate slenderness value $\lambda_{lim} = (b/t)(f_y/E)^{0.5}$ was used as a standardised form, the transformed yield slenderness limits are provided in Table 4. After transformation, similar and close yield slenderness limits are derived from EN 1993-1-12, AISC 360-16 and AS 4100 with 1.405, 1.400 and 1.414 respectively and relatively smaller magnitude of 1.280 is provided from AISI S100-16 and AS/NZS 4600. The Eurocode of EN 1993-1-5 [60] specifies the effective width equations with cross-section slenderness limit of $\bar{\lambda}_p = 0.673$ stipulated for those Class 4 (Slender) sections subject to local buckling. The original dimension width b is thus reduced to the effective width of b_{eff}, leading to the effective compressive resistance becomes at $A_{eff}f_y$, where A_{eff} is the effective area of the section. Analogous to the EN 1993-1-5, the design codes of AISC 360-16 and AS 4100 also specify the design system to consider the sections experiencing local buckling, albeit the expressions are different with different boundaries limit.

In parallel with the assessment on design codes, design approaches such as DSM, CSM, and GSRM, were also assessed. Although cross-section classification is not necessary in design approaches such as DSM, CSM and GSRM, the slenderness limit of $\lambda_p = 0.77$ as the threshold value for conventional sections was also assessed for their accuracy and appropriateness to IHexHS. DSM specifies that cross-section with slenderness limit λ_p greater than 0.77 cannot reach the yield load, whereas limit value of 0.68 is provided by CSM. Note that the generalised cross-sectional slenderness $\bar{\lambda}_L$ is adopted by GSRM, with detailed determination summarised in Table 4 and the sub-section of 3.3.2. The design approach of GSRM provides relatively smaller yield limits with $\bar{\lambda}_L = 0.5$ (with $\lambda_{lim} = 0.945$) compared with the other design approaches and design codes. Based on the graphical comparison results, the normalised resistance value converges to the unity at a value (intersection with the unity) far smaller than the current codified slenderness in design codes and design approaches, as shown in Fig. 12. Note that the distinct structural behaviours are caused by different aspect ratios. It can be concluded that the current stipulated slenderness limits were not suitable and cannot be extended to cover the cross-section classification of cold-formed HSS IHexHS. Similarly, the converted yield slenderness from the design approaches of DSM, CSM also show overly estimated cross-section classification, except for the GSRM, of which more accurate section yielding slenderness limit is specified. Based on regression analysis and graphical assessment, a new cross-section slenderness yield limit value of $\bar{\lambda}_p = 0.55$ ($\lambda_{lim} = 1.045$) is proposed for cold-formed HSS IHexHS under pure compression.

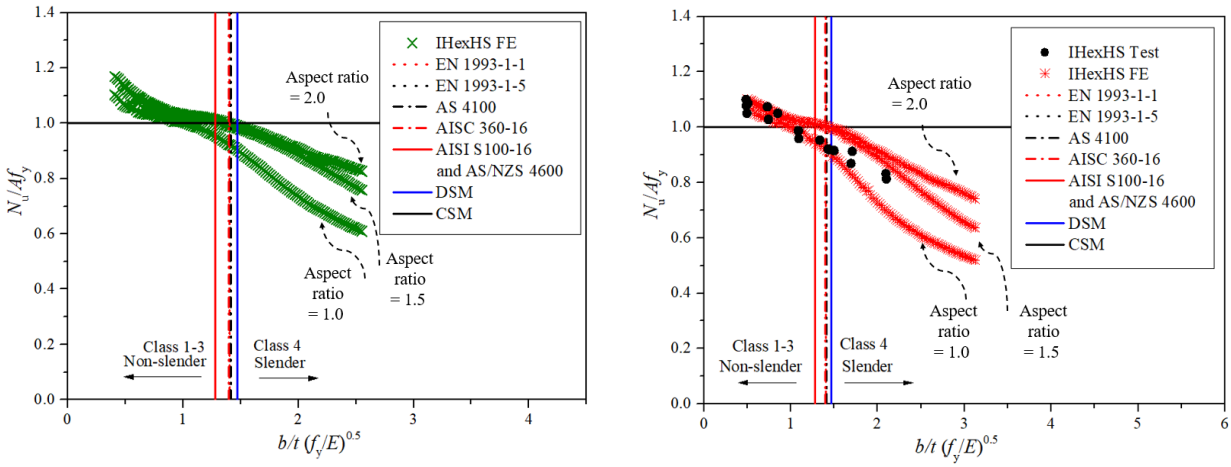

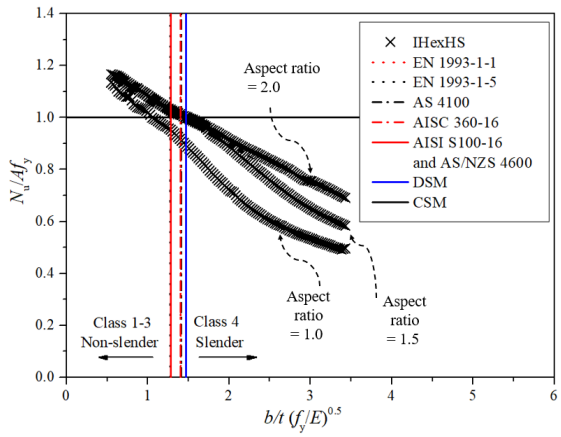

Fig. 12. Assessment of the cross-section classification yield limit from design codes and design approaches for cold-formed HSS IHexHS under pure compression (a) IHexHS with nominal yield strength of 460 MPa (b)

IHexHS with nominal yield strength of 690 MPa (c) IHexHS with nominal yield strength of 960 MPa.

Table 4 Summary of the cross-section yield slenderness limits for the internal plate element.

Design standards and methods	Yield slenderness limits	λ_{lim}
EN 1993-1-1	$b/t \leqslant 42\varepsilon_{EC3}$, $\varepsilon_{EC3}=\sqrt{235/f_y}$, $E = 210$ GPa	1.405
ANSI/AISC 360-16	$b/t \leqslant 1.40\varepsilon_{AISC}$, $\varepsilon_{AISC}=\sqrt{E/f_y}$, $E = 200$ GPa	1.400
EN 1993-1-5	$\overline{\lambda_p}=\frac{b/t}{28.4\varepsilon\sqrt{k}} \leq 0.5+\sqrt{0.085-0.055\psi}$, $\psi = 1$, $\varepsilon_{EC3}=\sqrt{235/f_y}$, $k = 4$, $E = 210$ GPa	1.279
AS 4100	$b/t \leqslant 14\varepsilon_{AS4100}$, $\varepsilon_{AS4100}=\sqrt{250/f_y}$, $E = 200$ GPa	1.414
AISI S100-16 AS/NZS	$\lambda_p=\sqrt{f_y/f_{cr}} \leq 0.673$, $f_{cr}=4\frac{\pi^2 E}{12(1-\nu^2)}(\frac{t}{b})^2$, $E = 200$ GPa	1.280
DSM	$\lambda_p=\sqrt{f_y/f_{cr}} \leq 0.776$, $E = 200$ GPa	1.470
CSM	$\lambda_p=\sqrt{f_y/f_{cr}} \leq 0.68$, $E = 200$ GPa	1.290
GSRM	$\overline{\lambda}_L=\sqrt{R_{pl}/R_{cr,L}}$, $\overline{\lambda}_L \leq 0.5+\sqrt{0.25-A}$, $A=0.225+0.025\psi_2\frac{1+\psi_1}{2}$, with $\psi_1=\psi_2=1$	0.945

3.3 Cross-sectional compression resistances

3.3.1 Assessment on design codes

Following the assessment of the cross-section classification, the evaluation of the design specifications for cross-sectional resistance under pure compression in design codes are presented in this section. As introduced in sub-sections of 3.1 and 3.2, the effective width method (EWM) is used in current design codes in EN 1993-1-5 [60], ANSI/AISC 360-16 [62], and AS 4100 [63] for cross sections subjected to local buckling failure prior to the attainment of yielding. Though the effective width concept used in structural steel design codes is currently applicable for traditional profile such as RHS/SHS, previous studies demonstrated that the plate buckling theory for the internal compression element in SHS/RHS can be extended to the internal plate members of OctHS/IOctHS [51, 52]. It is therefore considered to be suitable and applicable to extend and modify the EWM to IHexHS based on research data of the cross-section. The design formulae codified are briefly introduced and compared in this section. The effective width method and formulae given in EN 1993-1-5 [60] are as follows in Eqs. (3) – (4). The reduction of the whole area to the effective area of the slender plate elements is dependent on the boundary conditions, stress gradients, and dimensions.

$$\frac{b_{\text{eff,EC3}}}{b}=\begin{cases}1 & \text{for } \bar{\lambda}_{\text{p}} \le 0.5+\sqrt{0.085-0.055\psi} \\ \dfrac{\bar{\lambda}_{\text{p}}-0.055(3+\psi)}{\bar{\lambda}_{\text{p}}^{\,2}} & \text{for } \bar{\lambda}_{\text{p}} > 0.5+\sqrt{0.085-0.055\psi}\end{cases} \tag{3}$$

where $\bar{\lambda}_{\text{p}}$ is the plate slenderness specified in accordance with EN 1993-1-5 [60], k_σ is the buckling factor taken as 4 for internal plate element in compression, ψ is the stress distribution factor with $\psi = 1$ for elements under pure compression.

$$\bar{\lambda}_{\text{p}}=\frac{b/t}{28.4\varepsilon_{\text{EC3}}\sqrt{k_\sigma}} \tag{4}$$

In the North American Specification ANSI/AISC 360-16 [62], cross sections in which the width-to-thickness ratio of any compression plate element is greater than the limiting width-to-thickness ratio are defined as slender sections. For axial compression members with slender plate elements, the cross-sectional resistance can be derived based on the effective width $b_{\text{eff,AISC}}$, as expressed by Eqs. (5)-7).

$$\frac{b_{\text{eff,AISC}}}{b}=\begin{cases}1 & \text{for } b/t \le \lambda_{\text{r}}\sqrt{\dfrac{F_y}{F_{\text{cr}}}} \\ (1-c_1\sqrt{\dfrac{F_{\text{el}}}{F_{\text{cr}}}})\sqrt{\dfrac{F_{\text{el}}}{F_{\text{cr}}}} & \text{for } b/t > \lambda_{\text{r}}\sqrt{\dfrac{F_y}{F_{\text{cr}}}}\end{cases} \tag{5}$$

$$F_{\text{el}}=(c_2\frac{\lambda_{\text{r}}}{b/t})^2 F_{\text{y}} \tag{6}$$

$$c_2=\frac{1-\sqrt{1-4c_1}}{2c_1} \tag{7}$$

λ_{r} is the limiting width-to-thickness ratio of the plate, F_{el} is the elastic local buckling stress of the uniform compression plate element, c_1 and c_2 are the effective width imperfection adjustment factors, for the cold-formed IHexHS sections, the $c_1 = 0.20$ and $c_2 = 1.38$ for walls of square and rectangular hollow sections were used. F_{cr} is the critical stress of the compression members with non-slender element sections which can be determined following Eq. (8).

$$F_{\text{cr}}=\begin{cases}(0.658^{\frac{F_y}{F_{\text{e}}}})F_{\text{y}} & \text{for } KL/\text{r} \le 4.71\sqrt{\dfrac{E}{F_y}} \\ 0.877F_{\text{e}} & \text{for } KL/\text{r} > 4.71\sqrt{\dfrac{E}{F_y}}\end{cases} \tag{8}$$

where K is the effective length factor, L is the member length, r is the radius of gyration about the bending axis, E is the elastic modulus of steel, F_{e} is the elastic critical stress of the compression member, $F_{\text{e}} = \pi^2 E/(KL/r)^2$. Substituting and arranging the above formulae, the effective width method in the form of the limiting width to thickness ratio $\lambda_{\text{p,AISC}}$ instead of plate slenderness can be derived, as follows, in Eq. (9).

$$\frac{b_{\text{eff,AISC}}}{b}=\frac{1.38\lambda_{\text{p,AISC}}}{\lambda}-\frac{0.38\lambda_{\text{p,AISC}}^{\,2}}{\lambda^2} \tag{9}$$

As for the Australian Standard of AS 4100 [63], the effective width $b_{\text{e,AS4100}}$ for slender sections failed due to

elastic local buckling under compression is used to determine the effective area A_{eff}. The effective width method stipulated in AS 4100 [63] uses material related coefficient of $\varepsilon_{AS4100} = (250/f_y)^{0.5}$ and width to thickness ratio b/t, as shown in Eq. (10).

$$\frac{b_{eff,AS4100}}{b} = \frac{40}{b/(t\varepsilon_{AS4100})} \tag{10}$$

As seen in Fig. 13, all design codes provide over-conservative predictions for the relatively stocky sections for all the investigated steel grades, as the sections are only considered to achieve the yield load without strain hardening development. For relatively slender sections, slightly over-predicted cross-section strengths were observed from the existing design standards of EN 1993-1-5 and AISC 360-16, whereas conservative predictions were provided by AS 4100. For sections with aspect ratio higher than 1.0, all the design codes generate over-conservative predictions, as those sections (with nominal aspect ratio of 1.5 and 2.0) largely benefit from the element interaction effect, showing highly increased cross-sectional increased resistances. For the sections with intermediate slenderness with λ_p ranging between 0.55 and 0.68, marked over-predicted resistances were obtained due to the inappropriate cross-section classification yield limits.

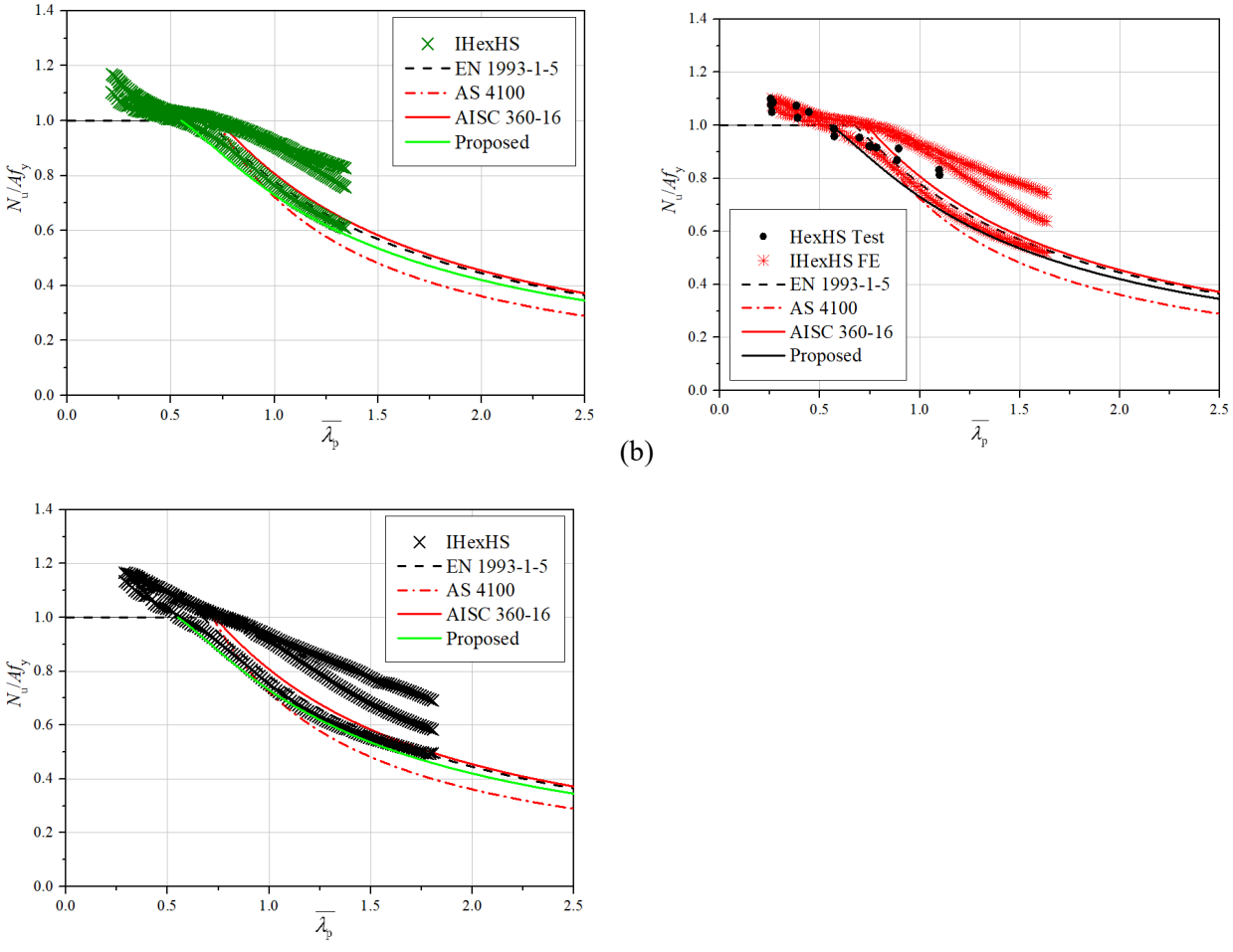

Fig. 13. Assessment of the effective width methods from design codes for cold-formed HSS IHexHS under pure compression (a) IHexHS with nominal yield strength of 460 MPa (b) IHexHS with nominal yield strength of 690 MPa (c) IHexHS with nominal yield strength of 960 MPa.

The normalised load ratio between ultimate resistance to the predictions is also plotted against the section slenderness in a form of $b/t\varepsilon$ as shown in Fig. 14 – Fig. 16. The mean values of $N_u/N_{u,pred}$ obtained from EC 3, AISC 360-16, AS4100 are 1.01, 1.00, and 1.03 with corresponding CoVs of 0.048, 0.059, and 0.037 respectively for sections with nominal yield strength of 460 MPa, and 0.99, 0.98, and 1.03 for sections with steel made from nominal yield strength of 690 MPa as shown in Table 5 – Table 7. For sections made of 960 MPa steel, the mean values of $N_u/N_{u,pred}$ are 1.00, 1.07, and 1.03 with corresponding CoVs of 0.067, 0.066, and 0.043 respectively for all the specimens. In general, design codes of EC 3 and AISC yield slightly unconservative predictions than AS 4100 for sections with aspect ratio of 1.0.and the unsafe predictions for slender section may lead to unsafe design which need to be improved.

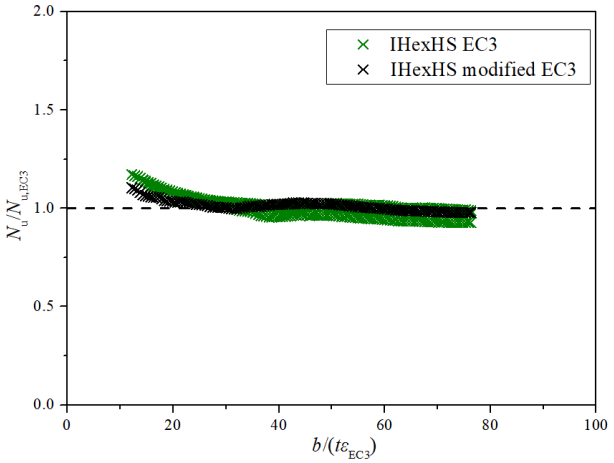

(a)

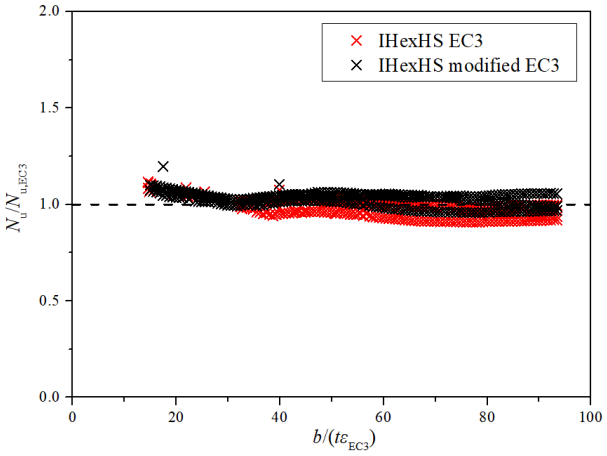

(b)

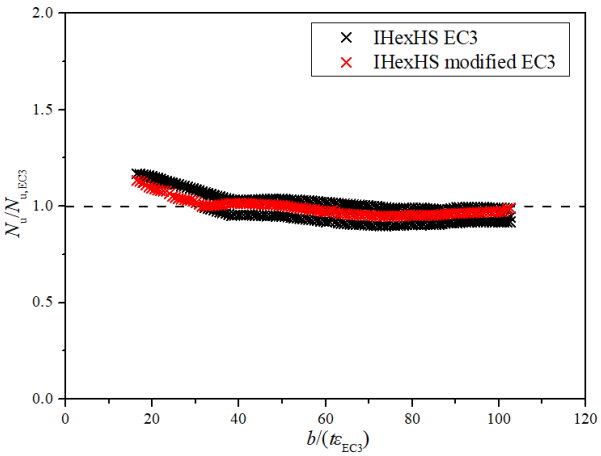

(c)

Fig. 14. Comparisons of experimental and numerical results with strength predictions from design code of Eurocode 3 for sections with nominal yield strength (a) 460 MPa (b) 690 MPa (c) 960 MPa.

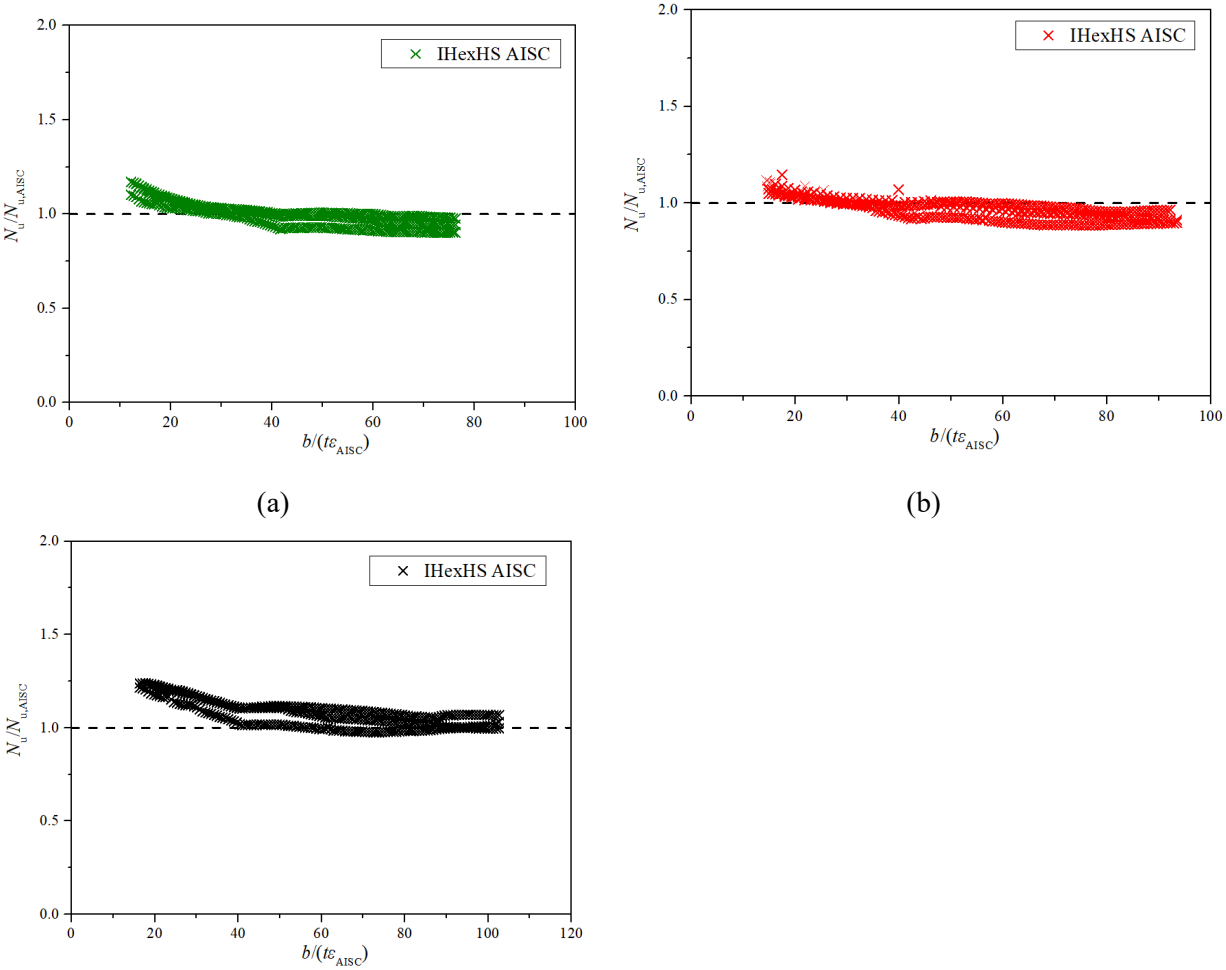

Fig. 15. Comparisons of experimental and numerical results with strength predictions from design code of AISC 360-16 for sections with nominal yield strength (a) 460 MPa (b) 690 MPa (c) 960 MPa.

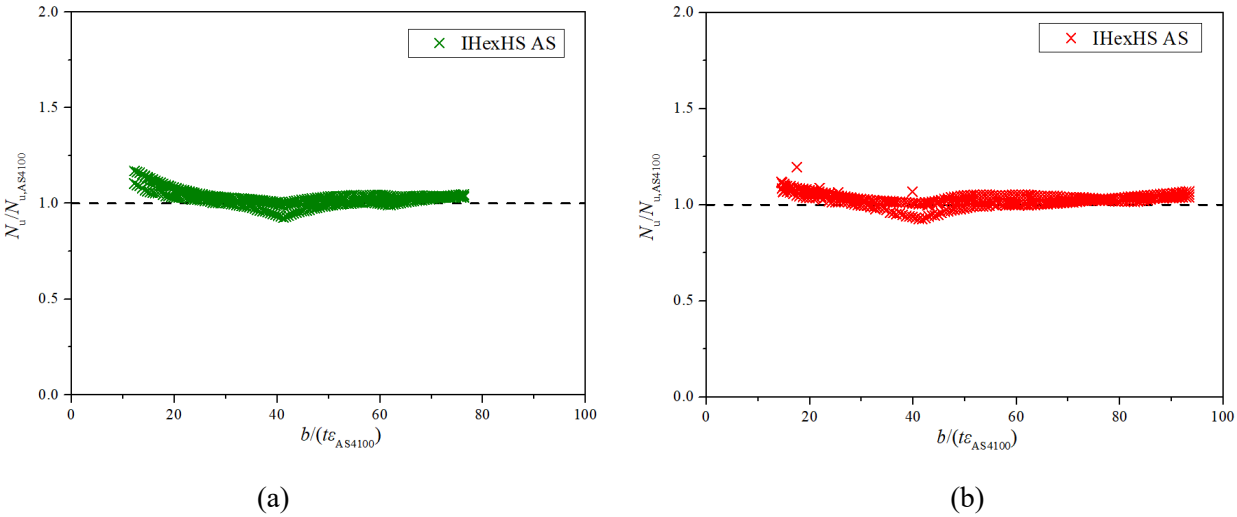

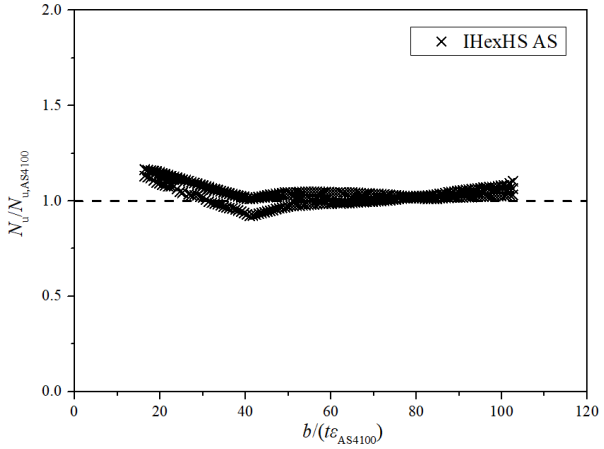

(c)

Fig. 16. Comparisons of experimental and numerical results with strength predictions from design code of AS 4100 for sections with nominal yield strength (a) 460 MPa (b) 690 MPa (c) 960 MPa.

3.3.2 Assessment on DSM, CSM, and GSRM

In addition to the design standards, design approaches of DSM, CSM and GSRM were also evaluated and developed for its application to cold-formed HSS IHexHS. It is known that these design approaches can be applicable to arbitrary cross sections without tedious procedure in finding the effective area of the buckled sections [73]. For design approach DSM, the sections can attain the yield load when the cross-section are smaller than $\lambda_p = 0.776$, for those sections with cross-section slenderness limit $\lambda_p \geq 0.776$, the predicted strength could be determined following the equation expressed by Eq. (11).

$$N_{DSM} = \begin{cases} f_y A & \text{for } \lambda_p \leq 0.776 \\ 1 - \frac{0.15}{\lambda_p^{0.8}} \frac{1}{\lambda_p^{0.8}} f_y A & \text{for } \lambda_p > 0.776 \end{cases} \quad (11)$$

Analogous to the DSM, design approach of CSM, accounting for the strain hardening of the metallic material and the effect of the element interaction, is developed based on the deformation capacity of the specimen. It replaces the traditional classification system with a continuous relationship between the section slenderness and deformation capacity [74, 75]. The CSM was originally developed mainly addressing for the strain hardening behaviour of stainless steel [76], extending to the design of carbon steel sections for both hot-rolled sections and cold-formed sections [77, 78] as well as hybrid sections [79]. To assess the strength predictions from CSM against the experimental and numerical results, the base curve developed by Lan et al. [80] available for the commonly used tubular sections SHS/RHS made from HSS were employed in this study, as given in Eq. (12). CSM material model for HSS cold-formed steel proposed by Buchanan et al. [81] was adopted.

$$\begin{cases} \frac{\varepsilon_{csm}}{\varepsilon_y} = \frac{0.294}{\lambda_p^{3.174}} \leq \min(15, \frac{C_1 \varepsilon_u}{\varepsilon_y}) & \text{for } \lambda_p \leq 0.68 \\ \frac{\varepsilon_{csm}}{\varepsilon_y} = (1 - \frac{0.219}{\lambda_p^{1.014}}) \frac{1}{\lambda_p^{1.014}} & \text{for } \lambda_p > 0.68 \end{cases} \quad (12)$$

where $(\varepsilon_{csm}/\varepsilon_y)$ is the deformation capacity, ε_{csm} is the CSM limiting strain, ε_y is the yield strain equals to f_y/E.

549
550 Two typical material model developed by Yun and Gardner [82] are applicabile to CSM design, (i) qual-linear
551 model for commonly used hot-rolled steels and (ii) bi-linear model which can represents the rounded response
552 of cold-formed steel, as shown in Fig. 17. To calculate the cross-section strength from CSM, the CSM limiting
553 stress f_{csm} needs to be derived based on CSM strbain. For quad-linear material model, the expressions given in
554 Eq. (13) originally developed for hot-rolled steel by Yun and Gardner [82] and bi-linear model employed in
555 [82] was used in this study, as shown in Eq. (14)
556

557
$$f_{csm}=\begin{cases} E_s\varepsilon_{csm} & \text{for } \varepsilon_{csm}\le\varepsilon_y \\ f_y & \text{for } \varepsilon_y<\varepsilon_{csm}<\varepsilon_{sh} \\ f_y+E_{sh}(\varepsilon_{csm}-\varepsilon_{sh}) & \text{for } \varepsilon_{sh}<\varepsilon_{csm}<C_1\varepsilon_u \end{cases} \quad (13)$$

558

559
$$f_{csm}=\begin{cases} E_s\varepsilon_{csm} & \text{for } \varepsilon_{csm}\le\varepsilon_y \\ f_y+E_{sh}(\varepsilon_{csm}-\varepsilon_{sh}) & \text{for } \varepsilon_y<\varepsilon_{csm}<C_1\varepsilon_u \end{cases} \quad (14)$$

560
561 where E_s is Young's modulus, f_y is the yield stress, ε_y and ε_u are the strains at the yield and ultimate stresses,
562 respectively, ε_{sh} is the strain hardening strain defined as the end of the yield plateau after which the strain
563 hardening initiates, $C_1\varepsilon_u$ represents the strain at the intersection point of the third stage of the model and the
564 actual stress-strain curve. Moreover, the other material coefficients C_2 is used to define the strain hardening
565 modulus of E_{sh}, as given in Eq. (15).
566
567 The hardening modulus of E_{sh} can be determined according to Eq. (16) with material coefficients C_2.

568
$$E_{sh}=\frac{f_u-f_y}{C_2\varepsilon_u-\varepsilon_y} \quad (15)$$

569 The numerical models with plates of nominal yield strength 460 MPa featured sharply defined yield plateau
570 for the material properties from flat portions, thus the quad-linear material model was used. For the corner
571 portions of 460 MPa steel plates and the both flat and corner portions of specimens with steel plates made of
572 690 MPa and 960 MPa, bi-linear material model was employed. The equation of cross-section strength from
573 CSM is as follows in Eq. (16),
574

575
$$N_{csm}=\begin{cases} f_{csm}A & \text{for } \lambda_p\le 0.68 \\ \dfrac{\varepsilon_{csm}}{\varepsilon_y}f_yA & \text{for } \lambda_p>0.68 \end{cases} \quad (16)$$

576 The design approach of generalised slenderness-based resistance method (GSRM) was developed to better
577 understand the structural behaviour of the commonly used hollow sections [83]. The developed approach was
578 originally developed with reference to the basic form of Winter's formulae with proposed design equations as
579 given in Eq. (17) and Eq. (18). The parameter A was calibrated to the results of the experimental and numerical
580 investigations. The calibrated parameter A is also correlated with the stress ratios Ψ_1 and Ψ_2, where Ψ_1 and Ψ_2
581 indicate the loading conditions with $\Psi_1 = \Psi_2 = 1.0$ for hollow sections under compression.

$$\frac{N_{GSRM}}{N_y}=\frac{1}{\lambda_L}\left(1-\frac{A}{\lambda_L}\right) \quad \text{for } \lambda_L \geq 0.5+\sqrt{0.25-A} \tag{17}$$

For cold-formed sections, the linear functions were determined through calibration as given in Eq. (18).

$$A=0.225+0.025\psi_2\frac{1+\psi_1}{2} \tag{18}$$

The comparisons implies that both DSM and GSRM provide over-conservative predictions for the relatively stocky sections for all the investigated steel grades, as the sections are only considered to achieve the yield load without strain hardening development, whereas the CSM generate more accurate results for stocky sections as anticipated since it can account for the materials strain hardening. For relatively slender sections, remarkedly over-predicted cross-section strengths were observed from the DSM, whereas close predictions were provided by CSM and GRSM. It should be noted that the discussions were evidenced and mainly focused on sections with nominal aspect ratio of 1.0. For sections failed due to elastic local buckling with nominal aspect ratio of 1.5 and 2.0, all design approaches yield over-conservative predictions as those sections were largely benefited from the constituent plate interaction effect, as shown in Fig. 18.

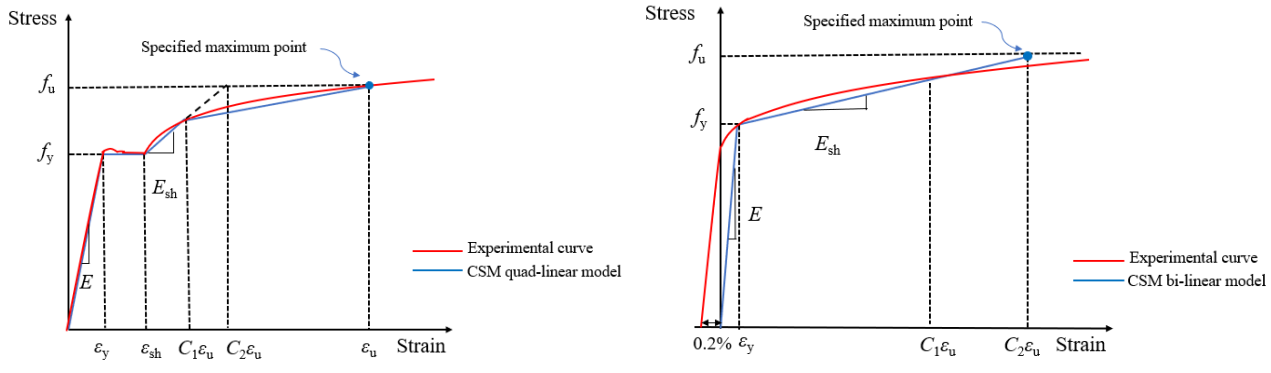

(a) (b)

Fig. 17. Material model for design approach of CSM (a) Qual-linear material model for stress-strain curve with yield plateau and sharply defined yield point (b) Bi-linear material model for stress-strain with typically rounded response without yeild plateau.

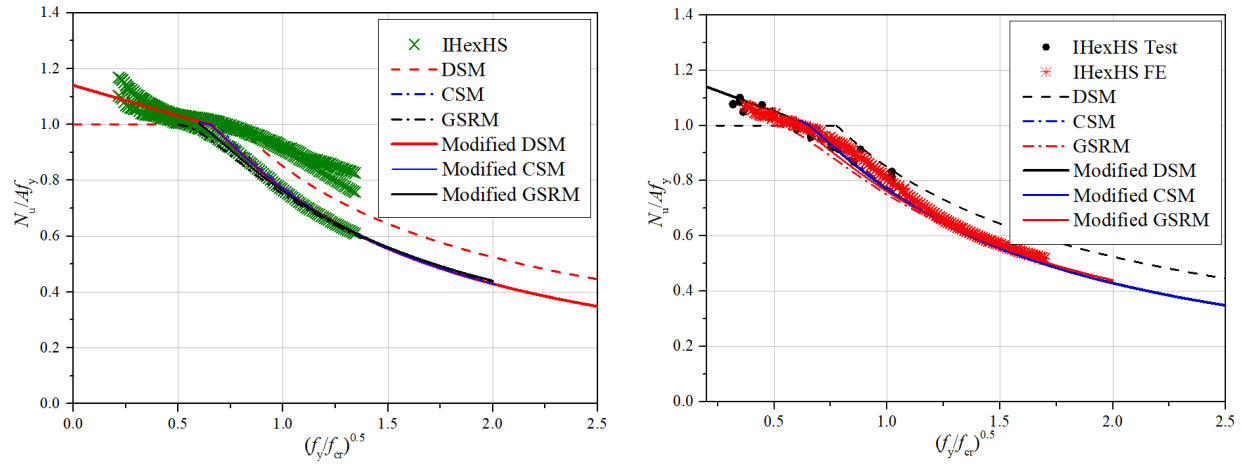

(a) (b)

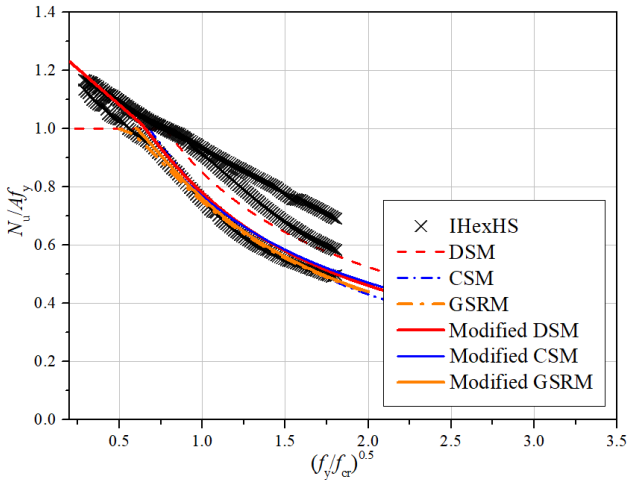

(c)

Fig. 18. Assessment of the design approaches for cold-formed HSS IHexHS under pure compression (a) IHexHS with nominal yield strength of 460 MPa (b) IHexHS with nominal yield strength of 690 MPa (c) IHexHS with nominal yield strength of 960 MPa

The normalised ratio is plotted against the section slenderness in a form of λ_p as seen in Fig. 19 – Fig. 21. The mean values of $N_u/N_{u,pred}$ obtained from design approaches of DSM, CSM, and GSRM for Q460 sections are 1.01, 1.06, and 1.09 with corresponding CoVs of 0.056, 0.049, and 0.056 respectively. The mean values of $N_u/N_{u,pred}$ for sections with nominal aspect ratio of 1.0 are 0.97, 1.02, and 1.05 with CoVs of 0.060, 0.015 and 0.041 respectively, as presented in Table 5 - 7. The graphical comparison further elucidates and evidences the conservate results of DSM for stocky sections (aspect ratio = 1.0) and unsafe predictions for slender sections (aspect ratio = 1.0). In comparison to DSM, CSM and GSRM provide more accurate predictions for slender sections as shown in Fig. 18. For sections with nominal aspect ratio of 1.0, the unsafe predictions from DSM for slender section will lead to unsafe design, underlying the necessities to modify the current DSM design formulae.

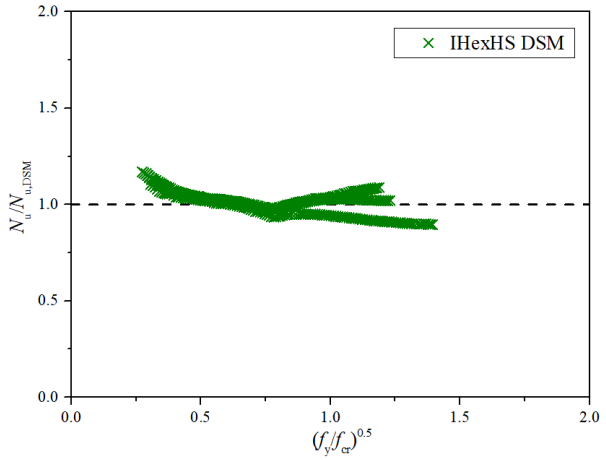

(a)

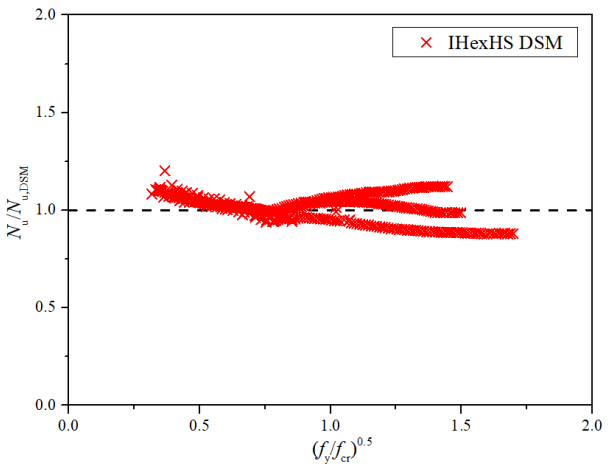

(b)

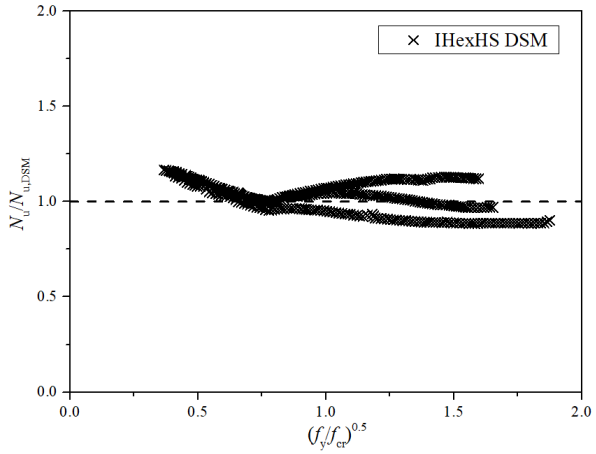

(c)

Fig. 19. Comparisons of experimental and numerical results with strength predictions from design approach of DSM for sections with nominal yield strength (a) 460 MPa (b) 690 MPa (c) 960 MPa

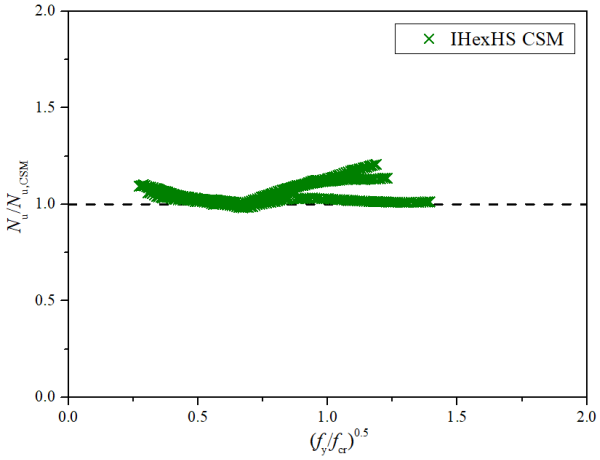

(a)

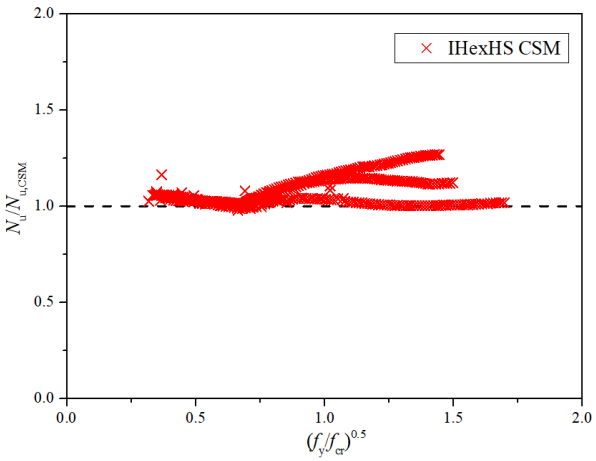

(b)

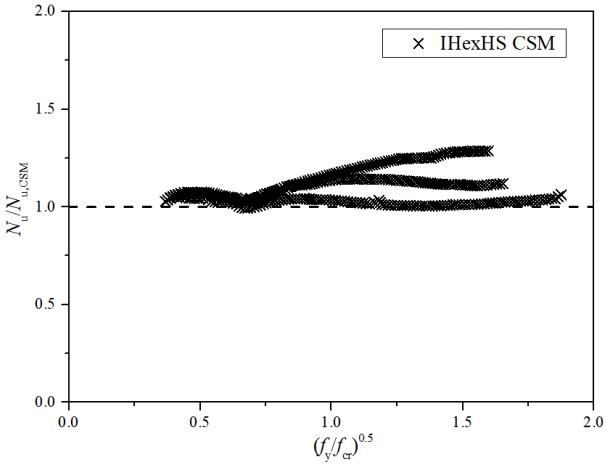

(c)

Fig. 20. Comparisons of experimental and numerical results with strength predictions from design approach of CSM for sections with nominal yield strength (a) 460 MPa (b) 690 MPa (c) 960 MPa

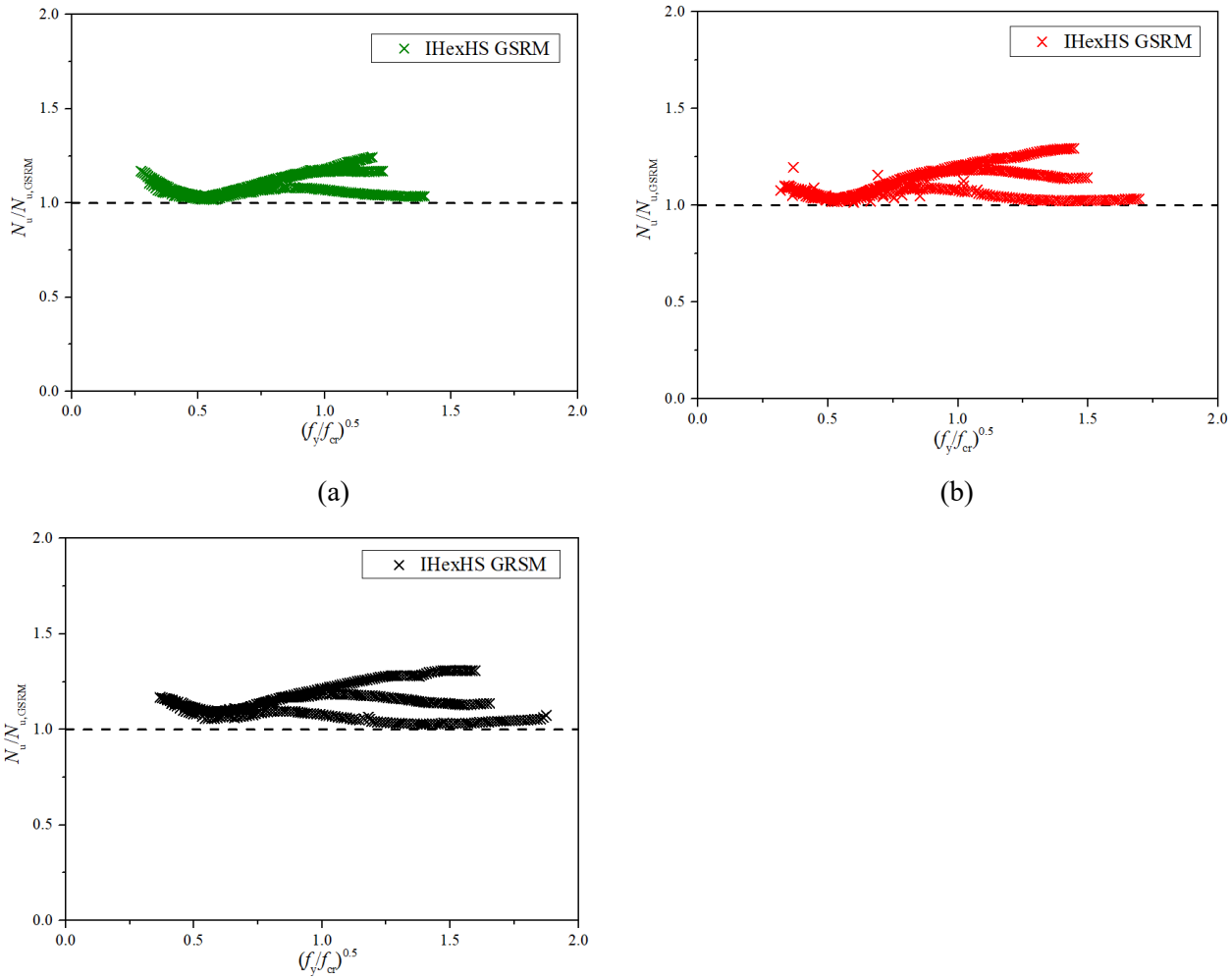

Fig. 21. Comparisons of experimental and numerical results with strength predictions from design approach of GSRM for sections with nominal yield strength (a) 460 MPa (b) 690 MPa (c) 960 MPa

4. Modifications on current design rules and design approaches

4.1 Modified Eurocode 3 (EC3)

The evaluation of the EWM reveal either unconservative or conservative predictions were obtained for the investigated specimens. As the concept of the effective width method is adopted in all structural steel design codes, improvements are mainly made with the focus on EC 3 specifications. It is of worthy noted that slender sections exhibit similar structural behaviour irrespective of steel grades as shown in Fig. 22 whereas the distinctions are observed for stocky sections with strain hardening due to the different material properties. Design modifications based on effective width from EN 1993-1-5 is developed and proposed in this section. The coefficients were modified based on regression analysis focusing on sections with aspect ratio of 1.0 as lower bound, with design formulae shown in Eq. (19).

$$\frac{b_{\text{eff,EC3}}}{b}=\begin{cases}1 & \text{for } \overline{\lambda}_{\text{p}} \le 0.5+\sqrt{0.058-0.055\psi} \\ \dfrac{0.95\overline{\lambda}_{\text{p}}-0.055(3+\psi)}{\overline{\lambda}_{\text{p}}^{\,2}} & \text{for } \overline{\lambda}_{\text{p}} > 0.5+\sqrt{0.058-0.055\psi}\end{cases} \tag{19}$$

The proposed design formulae with modified coefficients are plotted in Fig. 13 in line with the original effective width curve stipulated in design codes for various steel grades with notified improvement. Based on the modified formulae, the mean values of $N_{\text{u}}/N_{\text{u,EC3}}^{*}$ are 1.00, 1.00 and 1.00 with corresponding CoVs 0.038, 0.037, and 0.047 respectively for steel grades of 460 MPa, 690 MPa and 960 MPa respectively, as shown in Table 5 – Table 7. It should be noted that the original EWM provides conservative predictions for stocky sections as the strain hardening effect is not accounted for whereas overly-predicted cross-sectional resistance are obtained for slender sections. Therefore, the relatively higher normalised load ratio of $N_{\text{u}}/N_{\text{pred}}$ counteracted with the lower one, leading to somehow neutralised value with mean value much closer to the unity.

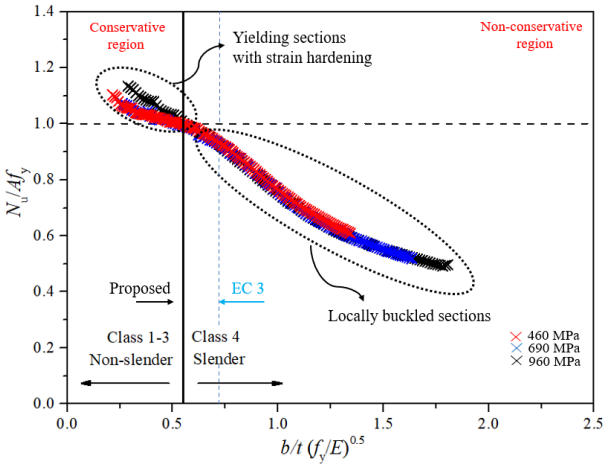

Fig. 22. Comparison of the normalised resistance between experimental (numerical) tested results to yield load with various steel grades.

4.2 Modified DSM

For the original DSM design provisions specified in AISI S100-16 [71], no consideration was made for the effect of the material strain hardening for sections undergoing significant plastic deformation, of which strain has developed into hardening stage, particularly for cold-formed stub column sections. To improve the design predictions for stocky sections, new formulae are proposed to tackle the great degree of conservatism by replacing the original horizontal yield limit with a linear expression comprising sections slenderness, and correlated factors to account for the material characteristics, as given in Eq. (20).

$$\frac{N_{\text{DSM}}}{N_{\text{y}}}=\begin{cases}1+(1-d_1\lambda_{\text{p}})d_2 & \text{for } \lambda_{\text{p}} \le 0.650 \\ (1-\dfrac{0.23}{\lambda_{\text{p}}^{\,0.901}})\dfrac{1}{\lambda_{\text{p}}^{\,0.901}} & \text{for } \lambda_{\text{p}} > 0.650\end{cases} \tag{20}$$

where the material coefficients of d_1 and d_2 are used to account for the effect of the strain hardening of the used material. Based on regression analysis the coefficients of d_1 and d_2 are equal to 1.6 and 0.18 for steel grades of

460 and 690, whereas $d_1 = 1.5$ and $d_2 = 0.33$ is proposed for sections with 960 MPa steel plates.

The normalised cross-sectional resistances are plotted against the sectional slenderness λ_p, as shown in Fig. 23. The mean values of $N_u/N_{u,DSM}^*$ for sections with steel grades of 460 MPa, 690 MPa and 960 MPa are 1.01, 1.01, and 1.01 respectively, and the corresponding values of CoV are 0.038, 0.037, and 0.036 respectively. Recall that the statistical analysis was conducted for both all thecc specimens and sections with aspect ratio of 1.0. The results show that the improved accuracy of the predictions is evidenced by the mean values of the experimental and numerical strength over the corresponding predicted strength ratio being closer to the unity and the possession of lower values of CoV.

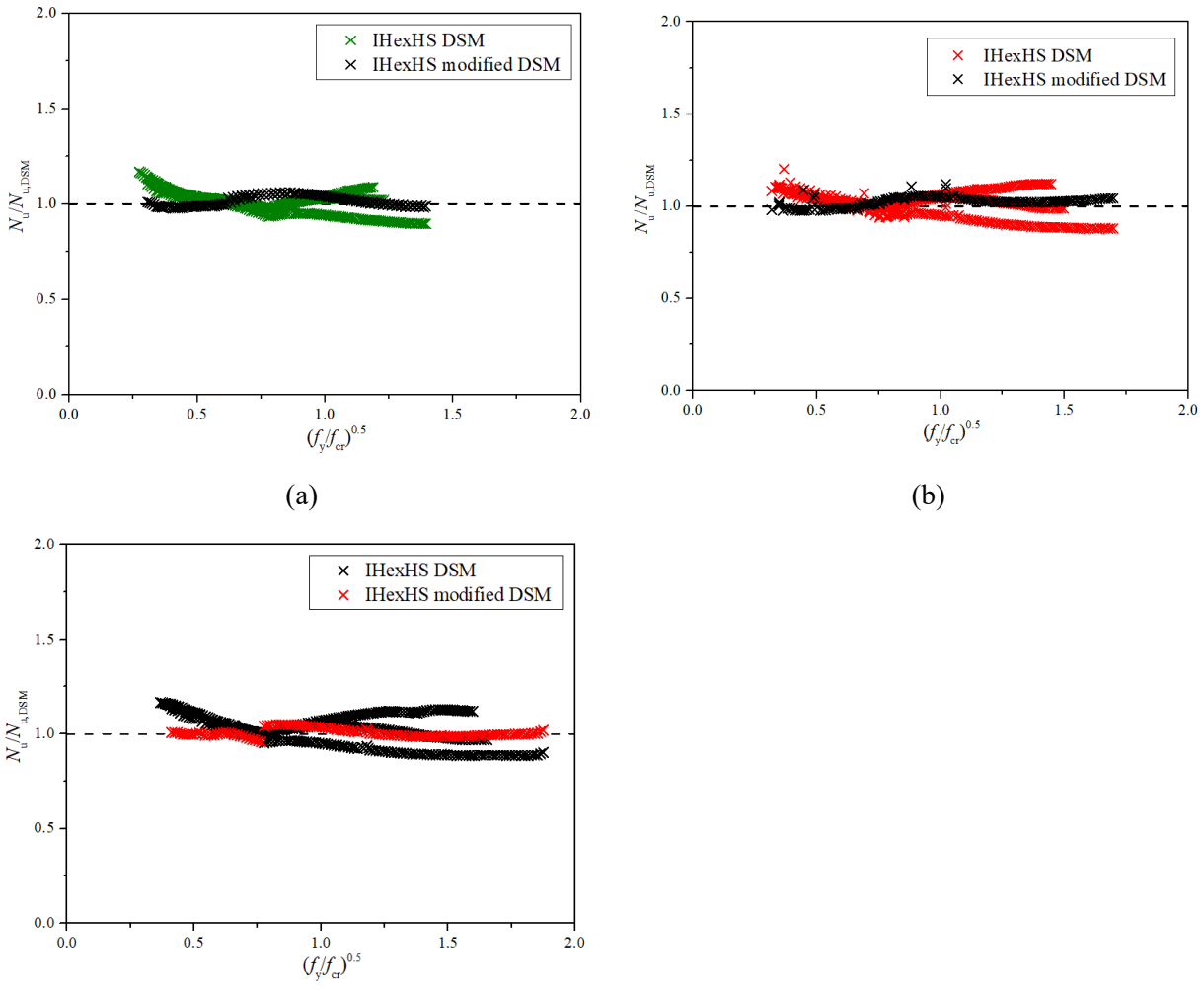

Fig. 23. Comparisons of experimental and numerical results with strength predictions from modified design approach of DSM for sections with nominal yield strength (a) 460 MPa (b) 690 MPa (c) 960 MPa

4.3 Modified CSM

The current base curve adopted in CSM is mainly developed based on the database of conventional tubular profile as discussed in the sub-section 3.3.2. The applicability of the existing base curve to the cold-formed HSS IHexHS is questionable, which need to be thoroughly investigated. The CSM base curve for the cold-

formed HSS HexHS is proposed and plotted with the base curve developed for both normal strength steel and high strength steel in Fig. 24.

$$\begin{cases} \dfrac{\varepsilon_{csm}}{\varepsilon_y} = \dfrac{0.257}{\lambda_p^{2.747}} \le \min(15, \dfrac{C_1\varepsilon_u}{\varepsilon_y}) & \text{for } \lambda_p \le 0.61 \\ \dfrac{\varepsilon_{csm}}{\varepsilon_y} = (1 - \dfrac{0.23}{\lambda_p^{0.901}}) \dfrac{1}{\lambda_p^{0.901}} & \text{for } \lambda_p > 0.61 \end{cases} \quad (21)$$

The material models, applicable to HSS cold-formed steel provided in [81, 84] were used and compared with the adopted material properties. It is noteworthy that the developed material models lack the development of corner portions due to the very limited data, thus leading to improper presentation of corner section material features, particularly for 960 MPa steel members, as shown in Fig. 25. The hot-rolled model proposed by Yun and Gardner [82] yields slightly over-estimated hardening strain. Nevertheless, the degree of the hardening is comparable to the adopted materials. The CSM curve is thereby improved by shifting the commencing point of hardening to the tested magnitudes with hardening slope remain unchanged for flat portion of 460 MPa steel. No modifications were made to CSM material model for 690 MPa sections for both flat and corner portions. For sections with 960 MPa steel plates, the current material model under-estimated the degree of hardening which cannot capture the rounded response. Although the close ultimate strengths were derived, the effect of the under-estimation at early stage was non-negligible as numerous sections cannot reach the strain larger than 2%. Hence, modifications were made to the flat and corner portions models taking account of the reduced elongation and ductility due to press-braking for corner portions and the ultimate strain was reduced for flat portions to attain larger hardening stiffness. The normalised cross-sectional resistances are plotted against the sectional slenderness λ_p, as shown in Fig. 26. The mean values of $N_u/N_{u,CSM}^*$ for sections with steel grades of 460 MPa, 690 MPa and 960 MPa are 1.02, 1.02, and 1.02 respectively, and the corresponding values of CoV are 0.039, 0.031, and 0.025 respectively. The less scattered predictions are evidenced by smaller values of CoV compared with original CSM and the improved accuracy of the predictions.

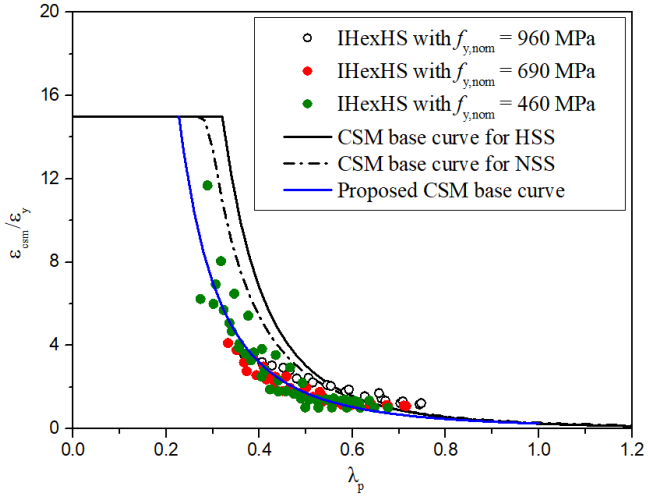

Fig. 24. Comparisons of proposed CSM base curve with the tested results.

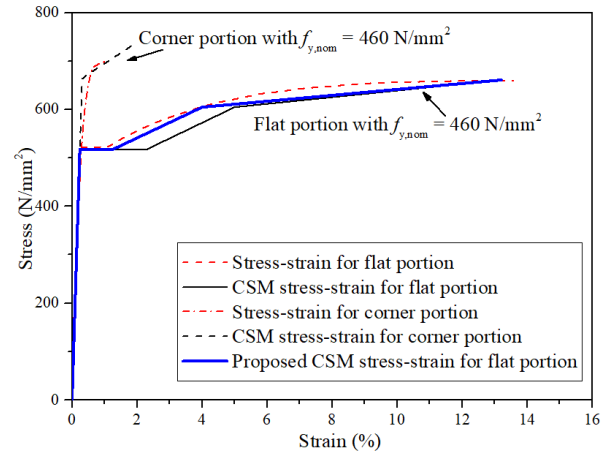

(a)

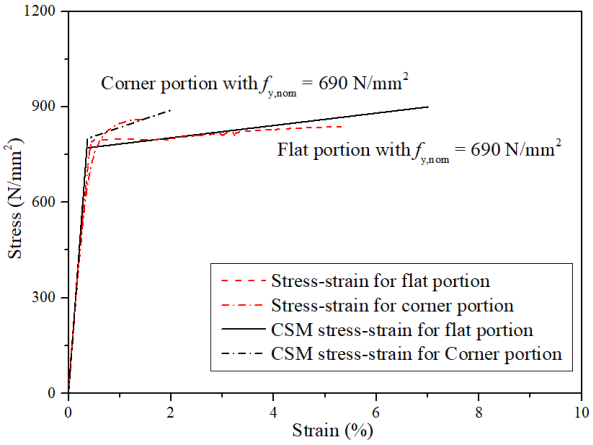

(b)

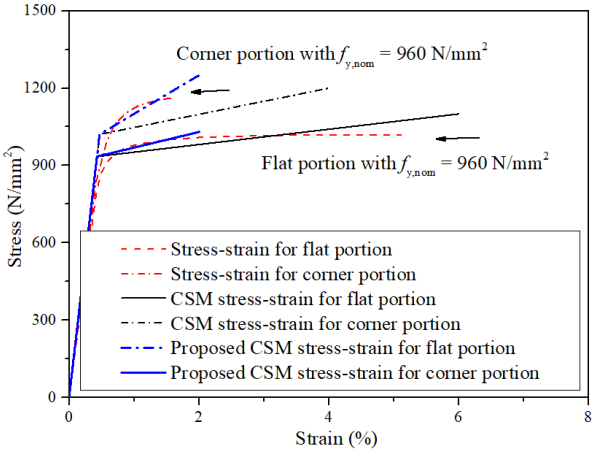

(c)

Fig. 25. Comparisons of stress-strain relationship for the material properties applied in CSM (a) sections with nominal yield strength of 460 MPa steel (b) sections with nominal yield strength of 690 MPa steel (c) sections with nominal yield strength of 960 MPa steel

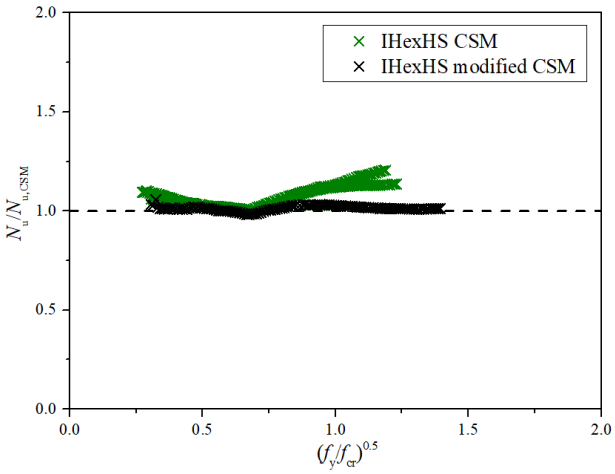

(a)

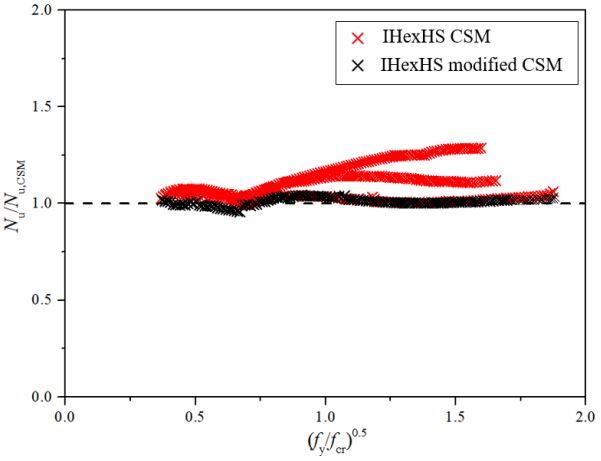

(b)

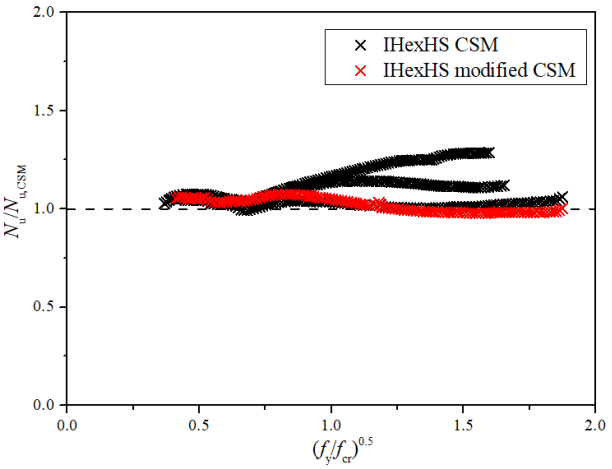

(c)

Fig. 26. Comparisons of experimental and numerical results with strength predictions from modified design approach of CSM for sections with nominal yield strength (a) 460 MPa (b) 690 MPa (c) 960 MPa

4.4 Modified GSRM

The modifications were also made to the design approach of GSRM based on the regression analysis with respect to the equation form of original GSRM with modified coefficients as follows given in Eq. (22)-Eq. (23). Improved accuracy can be observed in Fig. 27.

$$\frac{N_{GSRM}}{N_y}=\frac{1}{\lambda_L}\left(1-\frac{A}{\lambda_L}\right) \quad \text{for } \lambda_L \geq 0.5+\sqrt{0.25-A} \tag{22}$$

$$A=0.215+0.025\psi_2\frac{1+\psi_1}{2} \tag{23}$$

The normalised cross-sectional resistances are plotted against the sectional slenderness λ_p, as shown in Fig. 27. The mean values of $N_u/N_{u,GSRM}^*$ for sections (aspect ratio = 1.0) with steel grades of 460 MPa, 690 MPa and 960 MPa are 1.03, 1.03, and 1.04 respectively, which are closer to the unity compared with the original GSRM which provide 1.05, 1.05, and 1.06 respectively. The obtained corresponding values of CoV are 0.026, 0.024, and 0.023 respectively. The improvement of accuracy for the modified GSRM is also demonstrated by comparing the mean value of $N_u/N_{u,GSRM}^*$ for all the specimens, as detailed in Table 5 - Table 7.

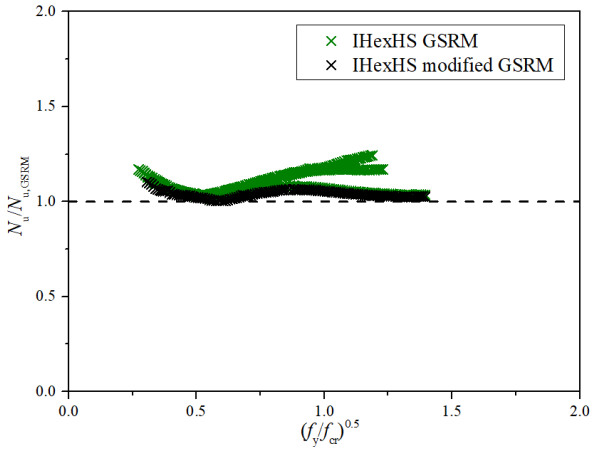

(a)

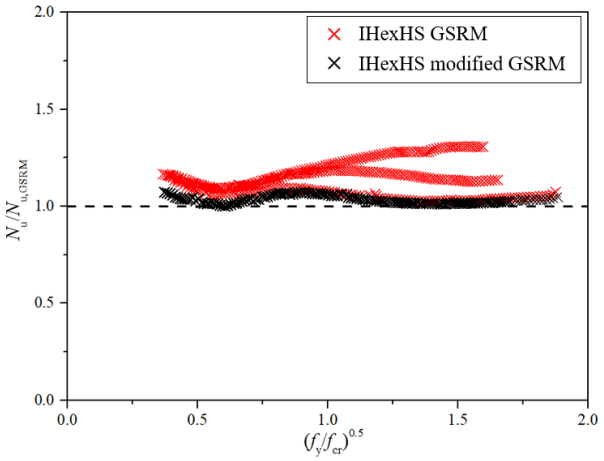

(b)

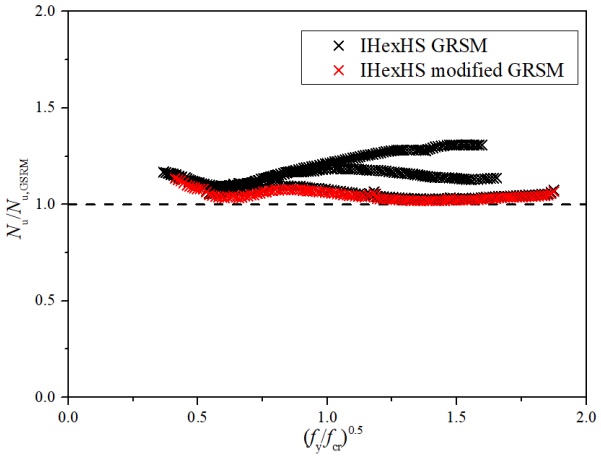

(c)

Fig. 27. Comparisons of experimental and numerical results with strength predictions from modified design approach of GSRM for sections with nominal yield strength (a) 460 MPa (b) 690 MPa (c) 960 MPa

Table 5 Comparisons of numerical results with predicted strengths based on different design methods for IHexHS with nominal yield strength of 460 MPa

No. of Specimen		N_u /$N_{u,EC3}$	N_u /$N_{u,AISC}$	N_u /$N_{u,AS4100}$	N_u /$N_{u,DSM}$	N_u /$N_{u,CSM}$	N_u /$N_{u,GSRM}$	N_u / $N_{u,EC3}^*$	N_u / $N_{u,DSM}^*$	N_u / $N_{u,CSM}^*$	N_u /$N_{u,GSRM}^*$
FE:450											
All data	Mean	1.01	1.00	1.03	1.01	1.06	1.09	1.03	1.08	1.08	1.11
	CoV	0.048	0.059	0.037	0.056	0.049	0.056	0.043	0.075	0.078	0.068
Subset:	Mean	0.98	0.97	1.01	0.97	1.02	1.05	1.00	1.01	1.02	1.03
AS = 1.0	CoV	0.050	0.063	0.038	0.060	0.015	0.041	0.038	0.038	0.039	0.026

Table 6 Comparisons of numerical results with predicted strengths based on different design methods for IHexHS with nominal yield strength of 690 MPa

No. of Specimen		N_u /$N_{u,EC3}$	N_u /$N_{u,AISC}$	N_u /$N_{u,AS4100}$	N_u /$N_{u,DSM}$	N_u /$N_{u,CSM}$	N_u /$N_{u,GSRM}$	N_u / $N_{u,EC3}^*$	N_u / $N_{u,DSM}^*$	N_u / $N_{u,CSM}^*$	N_u /$N_{u,GSRM}^*$
Test: 20 FE:450											
All data	Mean	0.99	0.98	1.03	1.01	1.08	1.11	1.03	1.07	1.07	1.10
	CoV	0.049	0.140	0.031	0.075	0.068	0.068	0.035	0.072	0.066	0.068
Subset:	Mean	0.96	0.95	1.01	0.96	1.02	1.05	1.00	1.01	1.02	1.03
AS = 1.0	CoV	0.055	0.067	0.038	0.095	0.015	0.024	0.037	0.037	0.031	0.024

Table 7 Comparisons of numerical results with predicted strengths based on different design methods for IHexHS with nominal yield strength of 960 MPa

No. of Specimen		N_u /$N_{u,EC3}$	N_u /$N_{u,AISC}$	N_u /$N_{u,AS4100}$	N_u /$N_{u,DSM}$	N_u /$N_{u,CSM}$	N_u /$N_{u,GSRM}$	N_u / $N_{u,EC3}^*$	N_u / $N_{u,DSM}^*$	N_u / $N_{u,CSM}^*$	N_u /$N_{u,GSRM}^*$
FE: 450											
All data	Mean	1.00	1.07	1.03	1.02	1.09	1.14	1.03	1.08	1.08	1.12
	CoV	0.067	0.066	0.043	0.076	0.071	0.068	0.050	0.077	0.071	0.069
Subset:	Mean	0.96	1.03	1.02	0.96	1.03	1.06	1.00	1.01	1.02	1.04
AS = 1.0	CoV	0.067	0.062	0.047	0.074	0.021	0.024	0.047	0.036	0.025	0.023

5. Reliability analysis

Reliability analysis was conducted in compliance with EN 1990 [85] to quantitatively assess the reliability level and required partial factor for existing design codes, design approaches, and proposed modified design approaches for cold-formed HSS IHexHS stub columns under concentric compression. The variability parameters (i.e., the ratio between the mean and nominal values X_m/X_n, where X represents the basic variables, and the corresponding CoV) of the basic material and geometric properties, where taken in accordance with Annex E of prEN 1993-1-1 [87]. The material over-strength ratio $f_{y,mean}/f_{y,nom}$ = 1.15 was used for HSS Q460 and $f_{y,mean}/f_{y,nom}$ = 1.10 was used for sections with 690 MPa and 960 MPa steel plates, with corresponding CoVs of 0.045 and 0.035 respectively [87]. The CoV of the geometric properties were taken as 0.009 and 0.025 for width and thickness respectively. The correction factor b can be derived based on least squares analysis between the resistance capacities from tests and design predictions from resistance model, as shown in Eq. (24), where r_e is the experimental results and r_t is the theoretical results of the resistance model.

$$b = \frac{\sum r_e r_t}{\sum r_t^2} \tag{24}$$

V_δ is the CoV of the FE results relative to the resistance design model, which can be determined as follows, in Eqs. (25) – (26).

$$V_\delta = \sqrt{\exp(s_\Delta{}^2) - 1} \tag{25}$$

$$s_\Delta{}^2 = \frac{1}{n-1}\sum_{i=1}^{n}(\Delta_i - \frac{1}{n}\sum_{i=1}^{n}\Delta_i)^2 \tag{26}$$

$$s_\Delta{}^2 = \ln(\delta_i) \tag{27}$$

where δ is the error term which is calculated for each pair data $\delta = r_e / b r_t$.

The effect of the variability of the geometric and material in resistance function $g_{rt}(X)$ are accounted for through their coefficient of variation parameter V_{rt}. The calculation of this parameter is shown in Eq. (28)

$$V_{rt} = \frac{VAR\left[g_{rt}(\underline{X})\right]}{g_{rt}{}^2(\underline{X}_m)} \cong \frac{1}{g_{rt}{}^2(\underline{X}_m)} \times \sum_{i=1}^{j}(\frac{\partial g_{rt}}{\partial X_i}\sigma_i)^2 \tag{28}$$

V_r is the combined CoV incorporating both model and basic variable uncertainties, and γ_{M0} is the partial safety factor for cross section resistance. To determine the partial safety factor, design resistance value needs to be derived as follows, in Eq. (29).

$$r_d = b g_{rt}(\underline{X}_m)\exp(-k_{d,\infty}\alpha_{rt}Q_{rt} - k_{d,n}\alpha_\delta Q_\delta - 0.5Q^2) \tag{29}$$

where $\alpha_{rt} = Q_{rt}/Q$, $\alpha_\delta = Q_\delta/Q$, $Q_{rt} = \sqrt{\ln(V_{rt}{}^2 + 1)}$, $Q_\delta = \sqrt{\ln(V_\delta{}^2 + 1)}$, and $Q = \sqrt{\ln(V_r{}^2 + 1)}$

The required partial safety factors, denoted as γ_{M0}, were calculated for the sections with different steel grades among 460 MPa, 690 MPa, and 960 MPa steel plates. For each considered steel grade, the dataset was divided further into subsets based on the aspect ratio of the cross-sections. The values of b, V_r and V_δ were determined for each subset and the detailed results of the statistical analysis are presented in Table 8 to Table 10. It is

concluded that the AS 4100 require lower partial factor than EC 3 and AISC 360-16 for all steel grades. With respect to the design approaches, CSM and GSRM provide the required partial factors close to the unity, indicating more reliable predictions than DSM, of which the most scattered predictions were obtained. The modified EC3 method generate improved reliability compared with the original one with reduced required partial factor. In terms of the design approaches, modified design formulae provide lower required partial factors for sections with aspect ratio of 1.0, primarily attributed to the lower values of the V_δ determined from modified methods, leading to notable improvement in cross-section predictions and increased consistency.

Table 8 Reliability analysis results for HSS IHexHS stub columns under concentric compression with nominal yield strength of 460 MPa.

Steel grade	No. of specimens		Design codes and design methods									
			EC3	AISC 360-16	AS 4100	DSM	CSM	GSRM	EC3*	DSM*	CSM*	GSRM*
Q460	All data: 470	$k_{d.n}$	3.116	3.116	3.116	3.116	3.116	3.116	3.116	3.116	3.116	3.116
		b	0.982	1.055	1.018	0.994	1.081	1.116	1.012	1.078	1.124	1.112
		V_δ	0.055	0.045	0.033	0.065	0.065	0.057	0.031	0.065	0.075	0.035
		V_r	0.063	0.055	0.046	0.093	0.072	0.065	0.044	0.072	0.081	0.047
		γ_{Mo}	1.133	1.026	1.031	1.153	1.060	1.003	1.032	1.063	1.050	0.948
Q460	Sub-set: 150 (AS= 1.0)	$k_{d.n}$	3.160	3.160	3.160	3.160	3.160	3.160	3.160	3.160	3.160	3.160
		b	1.012	1.027	1.002	0.926	1.006	1.038	0.982	1.006	1.005	1.031
		V_δ	0.048	0.058	0.032	0.087	0.016	0.026	0.027	0.023	0.016	0.025
		V_r	0.057	0.066	0.045	0.093	0.035	0.041	0.041	0.039	0.035	0.040
		γ_{Mo}	1.078	1.093	1.045	1.322	1.008	0.996	1.052	1.021	1.009	1.000

Table 9 Reliability analysis results for HSS IHexHS stub columns under concentric compression with nominal yield strength of 690 MPa.

Steel grade	No. of specimens		Design codes and design methods									
			EC3	AISC 360-16	AS 4100	DSM	CSM	GSRM	EC3*	DSM*	CSM*	GSRM*
Q690	All data: 470 Test: 20 FE:450	$k_{d.n}$	3.115	3.115	3.115	3.115	3.115	3.115	3.115	3.115	3.115	3.115
		b	0.973	1.048	1.021	0.982	1.077	1.112	1.018	1.075	1.112	1.108
		V_δ	0.048	0.036	0.029	0.076	0.066	0.067	0.033	0.071	0.067	0.050
		V_r	0.057	0.068	0.043	0.082	0.073	0.074	0.046	0.078	0.074	0.059
		γ_{Mo}	1.121	1.188	1.020	1.207	1.068	1.037	1.031	1.084	1.037	0.990
Q690	Sub-set: 150 (AS= 1.0)	$k_{d.n}$	3.160	3.160	3.160	3.160	3.160	3.160	3.160	3.160	3.160	3.160
		b	1.006	1.006	1.006	0.938	1.014	1.046	0.986	1.008	0.998	1.022
		V_δ	0.046	0.057	0.036	0.067	0.014	0.022	0.028	0.030	0.014	0.028
		V_r	0.056	0.065	0.048	0.074	0.035	0.038	0.042	0.044	0.035	0.042
		γ_{Mo}	1.079	1.113	1.050	1.229	0.998	0.980	1.053	1.033	1.014	1.015

Table 10 Reliability analysis results for HSS IHexHS stub columns under concentric compression with nominal yield strength of 960 MPa.

Steel grade	No. of specimens		Design codes and design methods									
			EC3	AISC 360-16	AS 4100	DSM	CSM	GSRM	EC3*	DSM*	CSM*	GSRM*
S960	All data: 450	$k_{d.n}$	3.116	3.116	3.116	3.116	3.116	3.116	3.116	3.116	3.116	3.116
		b	0.969	1.048	1.023	0.996	1.090	1.129	1.014	1.081	1.135	1.115
		V_δ	0.067	0.064	0.043	0.078	0.069	0.066	0.049	0.075	0.072	0.023
		V_r	0.074	0.071	0.066	0.084	0.076	0.074	0.059	0.081	0.078	0.039
		γ_{Mo}	1.188	1.090	1.094	1.194	1.065	1.019	1.080	1.092	1.030	0.921
S960	Sub-set: 150 (AS= 1.0)	$k_{d.n}$	3.160	3.160	3.160	3.160	3.160	3.160	3.160	3.160	3.160	3.160
		b	0.934	1.012	1.010	0.924	1.023	1.055	0.980	1.010	1.015	1.042
		V_δ	0.060	0.059	0.047	0.067	0.014	0.022	0.042	0.014	0.019	0.023
		V_r	0.068	0.067	0.057	0.074	0.035	0.039	0.053	0.035	0.035	0.039
		γ_{Mo}	1.208	1.111	1.077	1.248	0.989	0.972	1.097	0.936	0.997	0.985

6. Conclusions

A comprehensive numerical investigation into the local buckling behaviour and design of the cold-formed HSS IHexHS stub columns under concentric compression has been conducted and presented in this paper. The finite element models were developed firstly and validated against the experimental results for cold-formed HSS IHexHS. Extensive parametric studies were subsequently conducted using the validated FE models, covering a larger spectrum of sectional slenderness and steel grades. The obtained numerical results were then used to assess the accuracy and applicability of the current design codes of Eurocode 3, ANSI/AISC 360-16 and AS 4100 as well as the design approaches including DSM, CSM, and GSRM. Base on the results and discussions presented in this paper, the following conclusions can be made and summarised as follows:

(a) The current codified slenderness limits in the three structural steel design standards of EN 1993-1-1, AISC 360-16 and AS 4100 cannot be extended to cover the cross-section classification of cold-formed HSS IHextHS stub columns under compression. A new cross-section slenderness yield limit value of $\bar{\lambda}_{\mathrm{p}} = 0.55$ is proposed for cold-formed HSS IHexHS under pure compression.

(b) All design codes provide over-conservative predictions for stocky sections, and over-predicted cross-section resistances were provided from the existing design standards of EC3 and AISC 360-16 for slender sections, whereas conservative predictions were provided by AS 4100 for slender sections.

(c) Compared with design codes, design approach of CSM provide improved accuracy for both stocky and slender sections, principally due to the more suitable yield limits and the strain hardening effect is accounted for in strain-based design formulae.

(d) In comparison to design approach of DSM, CSM and GSRM provide more accurate predictions for slender sections, whereas CSM yield more accurate predictions for stocky sections.

(e) The modified design approaches of DSM, CSM, and GSRM provide more accurate and reliable design than the original design approaches. The modified DSM can take strain hardening into account, and the characteristics of the HSS material applicable to DSM need to be further developed.

Data Availability Statement

Some or all data that support the findings of this study are available from the corresponding author upon reasonable request.

Acknowledgement

The research work presented in this paper was supported by a grant from the Research Grants Council of the Hong Kong Special Administrative Region, China (Project no. 15218918). The authors would also like to thank the help from Dr. Shuai Li and Dr. Jiachen Guo.

References

927 [1] N. Baddoo, Briefing: More from less–greater materials efficiency using high-strength steels, Proc. Inst.
928 Civil Eng.-Struct. Build. 175(5) (2022) 359-362.
929 [2] O. Skoglund, J. Leander, R. Karoumi, Overview of steel bridges containing high strength steel, Int. J. Steel
930 Struct. 20(4) (2020) 1294-1301.
931 [3] T. Usami, Y. Fukumoto, Local and overall buckling of welded box columns, J. Struct. Div. 108(3) (1982)
932 525-542.
933 [4] M. Clarin, High strength steel: local buckling and residual stresses, Luleå tekniska universitet, 2004.
934 [5] L. Gao, H. Sun, F. Jin, H. Fan, Load-carrying capacity of high-strength steel box-sections I: Stub columns,
935 J. Constr. Steel. Res. 65(4) (2009) 918-924.
936 [6] D.-K. Kim, C.-H. Lee, K.-H. Han, J.-H. Kim, S.-E. Lee, H.-B. Sim, Strength and residual stress evaluation
937 of stub columns fabricated from 800MPa high-strength steel, J. Constr. Steel. Res. 102 (2014) 111-120.
938 [7] H. Ban, G. Shi, Y. Shi, Y. Wang, Overall buckling behavior of 460 MPa high strength steel columns:
939 Experimental investigation and design method, J. Constr. Steel. Res. 74 (2012) 140-150.
940 [8] H. Ban, G. Shi, Overall buckling behaviour and design of high-strength steel welded section columns, J.
941 Constr. Steel. Res. 143 (2018) 180-195.
942 [9] G. Shi, W. Zhou, Y. Bai, C. Lin, Local buckling of 460 MPa high strength steel welded section stub columns
943 under axial compression, J. Constr. Steel. Res. 100 (2014) 60-70.
944 [10] G. Shi, W. Zhou, C. Lin, Experimental investigation on the local buckling behavior of 960 MPa high
945 strength steel welded section stub columns, Adv Struct Eng 18(3) (2015) 423-437.
946 [11] N. Schillo, M. Feldmann, Interaction of local and global buckling of box sections made of high strength
947 steel, Thin-Walled Struct. 128 (2018) 126-140.
948 [12] Y.-B. Wang, G.-Q. Li, S.-W. Chen, F.-F. Sun, Experimental and numerical study on the behavior of axially
949 compressed high strength steel box-columns, Eng. Struc. 58 (2014) 79-91.
950 [13] S.-D. Nie, S.-B. Kang, L. Shen, B. Yang, Experimental and numerical study on global buckling of Q460GJ
951 steel box columns under eccentric compression, Eng. Struc. 142 (2017) 211-222.
952 [14] S.-B. Kang, B. Yang, X. Zhou, S.-D. Nie, Global buckling behaviour of welded Q460GJ steel box columns
953 under axial compression, J. Constr. Steel. Res. 140 (2018) 153-162.
954 [15] T.J. Li, G.Q. Li, S.L. Chan, Y.B. Wang, Behavior of Q690 high-strength steel columns: Part 1:
955 Experimental investigation, J. Constr. Steel. Res. 123 (2016) 18-30.
956 [16] Z. Huang, D. Li, B. Uy, H.-T. Thai, C. Hou, Local and post-local buckling of fabricated high-strength
957 steel and composite columns, J. Constr. Steel. Res. 154 (2019) 235-249.
958 [17] H. Fang, T.M. Chan, Buckling resistance of welded high-strength-steel box-section members under
959 combined compression and bending, J. Constr. Steel. Res. 162 (2019). 105711.1-105711.11.
960 [18] D. Li, Z. Huang, B. Uy, H.-T. Thai, C. Hou, Slenderness limits for fabricated S960 ultra-high-strength
961 steel and composite columns, J. Constr. Steel. Res. 159 (2019) 109-121.
962 [19] A. Su, Y. Sun, Y. Liang, O. Zhao, Membrane residual stresses and local buckling of S960 ultra-high
963 strength steel welded I-section stub columns, Thin-Walled Struct. 161 (2021) 107497.
964 [20] Y. Sun, Y. Liang, O. Zhao, Testing, numerical modelling and design of S690 high strength steel welded I-
965 section stub columns, J. Constr. Steel. Res. 159 (2019) 521-533.
966 [21] J.O. Ferreira Filho, T. Tankova, H. Carvalho, C. Martins, L.S. da Silva, Experimental and numerical
967 flexural buckling resistance of high strength steel columns and beam-columns, Eng. Struc. 265 (2022) 114414.
968 [22] T.Y. Ma, Y.F. Hu, X. Liu, G.Q. Li, K.F. Chung, Experimental investigation into high strength Q690 steel
969 welded H-sections under combined compression and bending, J. Constr. Steel. Res. 138(nov.) (2017) 449-462.
970 [23] J. Wang, S. Afshan, N. Schillo, M. Theofanous, M. Feldmann, L. Gardner, Material properties and

971 compressive local buckling response of high strength steel square and rectangular hollow sections, Eng. Struc.
972 130 (2017) 297-315.
973 [24] M. Gkantou, M. Theofanous, N. Antoniou, C. Baniotopoulos, Compressive behaviour of high-strength
974 steel cross-sections, Proceedings of the Institution of Civil Engineers 170(sb11) (2017) 813-824.
975 [25] X. Meng, L. Gardner, Testing of hot-finished high strength steel SHS and RHS under combined
976 compression and bending, Thin-Walled Struct. 148 (2020) 106262.
977 [26] P. Pannuzzo, T.-M. Chan, Flexural behaviour of cold-formed steel square and rectangular hollow sections
978 with moderate heat-treatment, J. Constr. Steel. Res. 197 (2022) 107454.
979 [27] H.-X. Shen, K.-K. Xu, Z.-J. Nie, Testing of high strength steel welded thin-walled RHS subjected to
980 combined compression and bending, Thin-Walled Struct. 179 (2022) 109661.
981 [28] X.L. Zhao, Section capacity of very high strength (VHS) circular tubes under compression, Thin-Walled
982 Struct. 37(3) (2000) 223-240.
983 [29] H. Jiao, X.L. Zhao, Imperfection, residual stress and yield slenderness limit of very high strength (VHS)
984 circular steel tubes, J. Constr. Steel. Res. 59(2) (2003) 233-249.
985 [30] J.-L. Ma, T.-M. Chan, B. Young, Experimental Investigation on Stub-Column Behavior of Cold-Formed
986 High-Strength Steel Tubular Sections, J. Struct. Eng. 142(5) (2016) 04015174.
987 [31] J.L. Ma, T.M. Chan, B. Young, Design of Cold-Formed High-Strength Steel Tubular Stub Columns, J.
988 Struct. Eng. 144(6) (2018). 4018063.1.
989 [32] H. Fang, T.M. Chan, B. Young, Structural performance of cold-formed high strength steel tubular columns,
990 Eng. Struc. 177 (2018) 473-488.
991 [33] X. Meng, L. Gardner, Cross-sectional behaviour of cold-formed high strength steel circular hollow
992 sections, Thin-Walled Struct. 156 (2020) 106822.
993 [34] X. Meng, L. Gardner, Stability and design of normal and high strength steel CHS beam-columns, Eng.
994 Struc. 251 (2022) 113361.
995 [35] X. Yun, X. Meng, L. Gardner, Design of cold-formed steel SHS and RHS beam–columns considering the
996 influence of steel grade, Thin-Walled Struct. 171 (2022) 108600.
997 [36] T.M. Chan, L. Gardner, Compressive resistance of hot-rolled elliptical hollow sections, Eng. Struc. 30(2)
998 (2008) 522-532.
999 [37] T.M. Chan, L. Gardner, Bending strength of hot-rolled elliptical hollow sections, J. Constr. Steel. Res.
1000 64(9) (2008) 971-986.
1001 [38] T.M. Chan, L. Gardner, Flexural Buckling of Elliptical Hollow Section Columns, J. Struct. Eng. 135(5)
1002 (2009) 546-557.
1003 [39] M.-T. Chen, B. Young, Behavior of cold-formed steel elliptical hollow sections subjected to bending, J.
1004 Constr. Steel. Res. 158 (2019) 317-330.
1005 [40] M.-T. Chen, B. Young, Beam-column tests of cold-formed steel elliptical hollow sections, Eng. Struc. 210
1006 (2020) 109911.
1007 [41] M.-T. Chen, B. Young, Material properties and structural behavior of cold-formed steel elliptical hollow
1008 section stub columns, Thin-Walled Struct. 134 (2019) 111-126.
1009 [42] M.-T. Chen, M. Pandey, B. Young, Post-fire residual material properties of cold-formed steel elliptical
1010 hollow sections, J. Constr. Steel. Res. 183 (2021) 106723.
1011 [43] M.-T. Chen, B. Young, Cross-sectional behavior of cold-formed steel semi-oval hollow sections, Eng.
1012 Struc. 177 (2018) 318-330.
1013 [44] M.-T. Chen, B. Young, Beam-column design of cold-formed steel semi-oval hollow non-slender sections,
1014 Thin-Walled Struct. 162 (2021) 107376.

[45] M.-T. Chen, B. Young, Tests of Cold-Formed Steel Semi-Oval Hollow Section Members under Eccentric Axial Load, J. Struct. Eng. 146(4) (2020). 04020027.1-04020027.12.
[46] M.-T. Chen, M. Pandey, B. Young, Mechanical properties of cold-formed steel semi-oval hollow sections after exposure to ISO-834 fire, Thin-Walled Struct. 167 (2021) 108202.
[47] J.-z. Liu, H. Fang, S. Chen, T.-M. Chan, Material properties and residual stresses of high strength steel hexagonal hollow sections, J. Constr. Steel. Res. 190 (2022) 107061.
[48] J.-z. Liu, H. Fang, T.-M. Chan, Structural behaviour of high strength steel hexagonal hollow section stub columns under axial compression, Eng. Struc. 268 (2022) 114653.
[49] J.-z. Liu, H. Fang, T.-M. Chan, Investigations on material properties and residual stresses in cold-formed high strength steel irregular hexagonal hollow sections, Thin-Walled Struct. 176 (2022) 109220.
[50] J.-z. Liu, H. Fang, T.-M. Chan, Experimental investigations on material properties and stub column behaviour of high strength steel irregular hexagonal hollow sections, J. Constr. Steel. Res. 196 (2022) 107343.
[51] J. Chen, J.-Y. Zhu, T.-M. Chan, Experimental and numerical investigation on stub column behaviour of cold-formed octagonal hollow sections, Eng. Struc. 214 (2020) 110669.
[52] H. Fang, T.-M. Chan, B. Young, Behavior of Octagonal High-Strength Steel Tubular Stub Columns, J. Struct. Eng. 145(12) (2019). 04019150.
[53] J.Z. Liu, H. Fang, T.M. Chan, Experimental investigation on material properties and residual stresses in cold-formed high strength steel irregular octagonal hollow sections, J. Constr. Steel. Res. 191(107170) (2022) 107170.
[54] J.-z. Liu, H. Fang, T.-M. Chan, Experimental and numerical investigations on stub column behaviour of cold-formed high strength steel irregular octagonal hollow sections, Thin-Walled Struct. 180 (2022) 109770.
[55] H. Fang, T.-M. Chan, B. Young, Structural performance of concrete-filled cold-formed high-strength steel octagonal tubular stub columns, Eng. Struc. 239 (2021) 112360.
[56] Z.M. Dalia, A.K. Bhowmick, G.Y. Grondin, Local buckling of multi-sided steel tube sections under axial compression and bending, J. Constr. Steel. Res. 186 (2021) 106909.
[57] H. Fang, T.M. Chan, B. Young, Material properties and residual stresses of octagonal high strength steel hollow sections, J. Constr. Steel. Res. 148 (2018) 479-490.
[58] J. Chen, H. Liu, T.-M. Chan, Material properties and residual stresses of cold-formed octagonal hollow sections, J. Constr. Steel. Res. 170 (2020) 106078.
[59] National Annex to Eurocode 3: Design of steel structures - Part 1-1: General rules and rules for buildings. UK National Annex to EN 1993-1-1, 2015, BS, 2015.
[60] EN 1993-1-5, Eurocode 3: Design of Steel Structures – Part 1–5: Plated structural elements., European Committee for Standardization (CEN), Brussels, 2006.
[61] National Annex to Eurocode 3: Design of steel structures - Part 1-12: Additional rules for the extension of EN 1993 up to steel grades S 700. UK National Annex to EN 1993-1-12, 2008, BS, 2008.
[62] ANSI/AISC 360-16, Specification for Structural Steel Buildings, American Institute of Steel Construction (AISC), Chicago, 2016.
[63] AS 4100-1998(R2016), Steel structures (Reconfirmed 2016 Incorporating Amendment No.1), AS 4100, Australian Standard, Sydney, Australia, 2016.
[64] ABAQUS/Standard. Version 6.14-1, K. a. S. Hibbit, U.S.A.
[65] F. Wang, O. Zhao, B. Young, Testing and numerical modelling of S960 ultra-high strength steel angle and channel section stub columns, Eng. Struc. 204 (2020) 109902.
[66] T.-M. Chan, X.-L. Zhao, B. Young, Cross-section classification for cold-formed and built-up high strength carbon and stainless steel tubes under compression, J. Constr. Steel. Res. 106 (2015) 289-295.

[67] J.-z. Liu, S. Chen, T.-M. Chan, Testing, numerical modelling and design of Q690 high strength steel welded T-section stub columns, Eng. Struc. 259 (2022) 114142.
[68] J.-z. Liu, S. Chen, T.-M. Chan, Experimental and numerical investigations of hybrid high strength steel welded T-section stub columns with Q690 flange and Q460 web, Thin-Walled Struct. 177 (2022) 109403.
[69] L. Gardner, D.A. Nethercot, Numerical Modeling of Stainless Steel Structural Components—A Consistent Approach, J. Struct. Eng. 130(10) (2004) 1586-1601.
[70] T.G. Singh, K.D. Singh, Structural performance of YSt–310 cold–formed tubular steel stub columns, Thin-Walled Struct. 121 (2017) 25-40.
[71] AISI S100-16, North American Specification for the Design of Cold-Formed Steel Structural Members, AISI (American Iron and Steel Institute), Washington, DC, USA, 2016.
[72] AS/NZS 4600:2018, Cold-formed steel structures, AS/NZS 4600, Australian/New Zealand Standards, Sydney, Australia and Wellington, New Zealand, 2018.
[73] B.W. Schafer, Advances in the Direct Strength Method of cold-formed steel design, Thin-Walled Struct. 140 (2019) 533-541.
[74] L. Gardner, The continuous strength method, Proc. Inst. Civil Eng.-Struct. Build. 161(3) (2008) 127-133.
[75] S. Afshan, L. Gardner, The continuous strength method for structural stainless steel design, Thin-Walled Struct. 68 (2013) 42-49.
[76] O. Zhao, S. Afshan, L. Gardner, Structural response and continuous strength method design of slender stainless steel cross-sections, Eng. Struc. 140 (2017) 14-25.
[77] X. Yun, L. Gardner, Numerical modelling and design of hot-rolled and cold-formed steel continuous beams with tubular cross-sections, Thin-Walled Struct. 132 (2018) 574-584.
[78] X. Yun, L. Gardner, N. Boissonnade, The continuous strength method for the design of hot-rolled steel crosssections, Eng. Struc. 157 (2018) 179-191.
[79] J.-z. Liu, S. Chen, T.-M. Chan, Hybrid welded T-section stub columns with Q690 flange and Q355 web: Testing, modelling and design, Eng. Struc. 274 (2023) 115142.
[80] X. Lan, J. Chen, T.-M. Chan, B. Young, The continuous strength method for the design of high strength steel tubular sections in compression, Eng. Struc. 162 (2018) 177-187.
[81] C. Buchanan, L. Gardner, A. Liew, The continuous strength method for the design of circular hollow sections, J. Constr. Steel. Res. 118 (2016) 207-216.
[82] X. Yun, L. Gardner, Stress-strain curves for hot-rolled steels, J. Constr. Steel. Res. 133 (2017) 36-46.
[83] A. Toffolon, X. Meng, A. Taras, L. Gardner, The generalized slenderness-based resistance method for the design of SHS and RHS, Steel Construction 12(4) (2019) 327-341.
[84] L. Gardner, X. Yun, Description of stress-strain curves for cold-formed steels, Constr. Build. Mater. 189 (2018) 527-538.
[85] EN 1990. Eurocode - Basis of structural design, European Committee for Standardization (CEN), Brussels, Belgium, 2002.
[86] B. Somodi, B. Kövesdi, Flexural buckling resistance of cold-formed HSS hollow section members, J. Constr. Steel. Res. 128 (2017) 179-192.
[87] prEN1993-1-1.Eurocode 3: Design of Steel Structures – Part 1-1: General Rules and Rules for Buildings, Final document, European Committee for Standardization (CEN), Brussels, 2020.
[88] R.D. Ziemian, Guide to stability design criteria for metal structures, John Wiley & Sons2010.